

Gene Expression Analysis. TRIzol reagent (Invitrogen) was used to prepare total RNA from tissues. The reverse-transcription reaction was carried out with a high-capacity cDNA reverse transcription kit (Applied Biosystems). Quantitative PCR analyses using TaqMan assays were performed as previously described (37). The relative expression levels were normalized by measurement of the amount of cyclophilin in each sample.

Histological Analysis. Tissue samples for histology were fixed in 4% paraformaldehyde in PBS overnight, and paraffin-embedded sections were prepared (4- μ m sections). Sections of liver were stained with H&E, and adipose tissues were stained hematoxylin and incubated with anti-F4/80 (1:20; Serotec) overnight at 4 °C, followed by incubation with the Vectastain Elite ABC Rat IgG Kit and visualization with the ImmPACT DAB Substrate Kit (Vector Laboratories), as previously described (5).

Adipose Tissue Fractionation and FACS Analysis. Adipose tissue fractionation into the stromal vascular fraction (SVF) was performed as previously described (5). Briefly, epididymal adipose tissue pads were minced into fine pieces and centrifuged at 3,000 \times g to remove erythrocytes and free leukocytes. Tissues were incubated with 2 mg/mL of collagenase type 2 (Worthington) at 37 °C with gentle agitation for 15–20 min. Digested tissues were filtered through nylon mesh (100 μ m), and the filtrate was centrifuged at 1,200 \times g. Pelleted cells were collected as the SVF. For isolation of mRNA, the erythrocyte-depleted SVF was resuspended in TRIzol reagent (Invitrogen). For flow cytometric analysis, after removing red blood cells, the SVF was incubated with either labeled monoclonal antibody or isotype control antibody and analyzed by flow cytometry using a FACS Calibur (Becton Dickinson). Data acquisition and analysis were performed using CellQuest Pro software (Becton Dickinson). Propidium iodide was used to exclude dead cells.

Plasma MCP-1 and Hepatic Triglyceride Content. Plasma levels for MCP-1 were measured by ELISA (R&D Systems). Hepatic triglyceride was extracted from

the liver homogenate with Folch solvent (chloroform:methanol = 2:1, vol/vol). An aliquot of the organic phase was collected and resuspended in ethanol containing 1% Triton X-100 and then measured by enzyme-based measurement kits (Roche Diagnostics).

Bone Marrow Transplantation. For BM transplant studies, bone marrow cells were prepared from the femur and tibia of *Pik3cg^{+/+}* and *Pik3cg^{-/-}* mice and injected i.v. (5×10^6 cells/recipient) into lethally irradiated *ob/ob* mice or C57BL/6J mice (7.0 Gy) as recipients, as described previously (39, 40).

Treatment with a PI3K γ Inhibitor. A PI3K γ selective inhibitor, AS-605240, which was synthesized by Discovery Research Laboratories, Kyorin Pharmaceutical, was used as described previously (25). Vehicle or AS-605240 was administered intraperitoneally to *ob/ob* mice twice a day from 6 wk of age.

Statistical Analysis. Values of the data are expressed as mean \pm SEM. Differences between two groups were assessed using unpaired two-tailed *t* tests. Data involving more than two groups were assessed by analysis of variance. Statistical significance is displayed as *P* < 0.05 (one asterisk) or *P* < 0.01 (two asterisks) in figures.

ACKNOWLEDGMENTS. We thank R. Hoshino, F. Takahashi, Y. Kanto, and Y. Kishida for their excellent technical assistance. This work was supported by a grant for the Translational Systems Biology and Medicine Initiative from the Ministry of Education, Culture, Sports, Science and Technology of Japan (to T.K.), a Grant-in-Aid for Scientific Research in Priority Areas (S) from the Ministry of Education, Culture, Sports, Science and Technology of Japan (to T.K.), a Grant-in-Aid for Scientific Research in Priority Areas (B) from the Ministry of Education, Culture, Sports, Science and Technology of Japan (to K.U.), a Grant-in-Aid for Scientific Research from the Ministry of Health, Labor and Welfare (to K.U.), Health Science Research grants (Research on Human Genome and Gene Therapy) from the Ministry of Health and Welfare (to T.K.), and a grant from Takeda Science Foundation (to K.U.).

- Kahn SE, Hull RL, Utzschneider KM (2006) Mechanisms linking obesity to insulin resistance and type 2 diabetes. *Nature* 444:840–846.
- Yach D, Stuckler D, Brownell KD (2006) Epidemiologic and economic consequences of the global epidemics of obesity and diabetes. *Nat Med* 12:62–66.
- Weisberg SP, et al. (2003) Obesity is associated with macrophage accumulation in adipose tissue. *J Clin Invest* 112:1796–1808.
- Xu H, et al. (2003) Chronic inflammation in fat plays a crucial role in the development of obesity-related insulin resistance. *J Clin Invest* 112:1821–1830.
- Kamei N, et al. (2006) Overexpression of monocyte chemoattractant protein-1 in adipose tissues causes macrophage recruitment and insulin resistance. *J Biol Chem* 281:26602–26614.
- Kanda H, et al. (2006) MCP-1 contributes to macrophage infiltration into adipose tissue, insulin resistance, and hepatic steatosis in obesity. *J Clin Invest* 116:1494–1505.
- Zeyda M, et al. (2007) Human adipose tissue macrophages are of an anti-inflammatory phenotype but capable of excessive pro-inflammatory mediator production. *Int J Obes (Lond)* 31:1420–1428.
- Chavey C, et al. (2009) CXC ligand 5 is an adipose-tissue derived factor that links obesity to insulin resistance. *Cell Metab* 9:339–349.
- Oak JS, Matheu MP, Parker I, Cahalan MD, Fruman DA (2007) Lymphocyte cell motility: The twisting, turning tale of phosphoinositide 3-kinase. *Biochem Soc Trans* 35:1109–1113.
- Hirsch E, et al. (2000) Central role for G protein-coupled phosphoinositide 3-kinase gamma in inflammation. *Science* 287:1049–1053.
- Sasaki T, et al. (2000) Function of PI3Kgamma in thymocyte development, T cell activation, and neutrophil migration. *Science* 287:1040–1046.
- Lumeng CN, Bodzin JL, Sattler AR (2007) Obesity induces a phenotypic switch in adipose tissue macrophage polarization. *J Clin Invest* 117:175–184.
- Lumeng CN, DelProposto JB, Westcott DJ, Sattler AR (2008) Phenotypic switching of adipose tissue macrophages with obesity is generated by spatiotemporal differences in macrophage subtypes. *Diabetes* 57:3239–3246.
- Gordon S (2003) Alternative activation of macrophages. *Nat Rev Immunol* 3:23–35.
- Nishimura S, et al. (2009) CD8+ effector T cells contribute to macrophage recruitment and adipose tissue inflammation in obesity. *Nat Med* 15:914–920.
- Després JP, Lemieux I (2006) Abdominal obesity and metabolic syndrome. *Nature* 444:881–887.
- Perlemuter G, Bigorgne A, Cassard-Doulcier AM, Naveau S (2007) Nonalcoholic fatty liver disease: From pathogenesis to patient care. *Nat Clin Pract Endocrinol Metab* 3:458–469.
- Tontonoz P, Spiegelman BM (2008) Fat and beyond: The diverse biology of PPARgamma. *Annu Rev Biochem* 77:289–312.
- Bouhrel MA, et al. (2007) PPARgamma activation primes human monocytes into alternative M2 macrophages with anti-inflammatory properties. *Cell Metab* 6:137–143.
- Odegaard JI, et al. (2007) Macrophage-specific PPARgamma controls alternative activation and improves insulin resistance. *Nature* 447:1116–1120.
- Matsusue K, et al. (2008) Hepatic steatosis in leptin-deficient mice is promoted by the PPARgamma target gene *Fsp27*. *Cell Metab* 7:302–311.
- Nishino N, et al. (2008) FSP27 contributes to efficient energy storage in murine white adipocytes by promoting the formation of unilocular lipid droplets. *J Clin Invest* 118:2808–2821.
- Tamura Y, et al. (2008) Inhibition of CCR2 ameliorates insulin resistance and hepatic steatosis in db/db mice. *Arterioscler Thromb Vasc Biol* 28:2195–2201.
- Yang SJ, Iglayreger HB, Kadouh HC, Bodary PF (2009) Inhibition of the chemokine (C-C motif) ligand 2/chemokine (C-C motif) receptor 2 pathway attenuates hyperglycaemia and inflammation in a mouse model of hepatic steatosis and lipodystrophy. *Diabetologia* 52:972–981.
- Barber DF, et al. (2005) PI3Kgamma inhibition blocks glomerulonephritis and extends lifespan in a mouse model of systemic lupus. *Nat Med* 11:933–935.
- Guillemet-Guibert J, et al. (2008) The p110beta isoform of phosphoinositide 3-kinase signals downstream of G protein-coupled receptors and is functionally redundant with p110gamma. *Proc Natl Acad Sci USA* 105:8292–8297.
- Camps M, et al. (2005) Blockade of PI3Kgamma suppresses joint inflammation and damage in mouse models of rheumatoid arthritis. *Nat Med* 11:936–943.
- Weisberg SP, et al. (2006) CCR2 modulates inflammatory and metabolic effects of high-fat feeding. *J Clin Invest* 116:115–124.
- Huber J, et al. (2008) CC chemokine and CC chemokine receptor profiles in visceral and subcutaneous adipose tissue are altered in human obesity. *J Clin Endocrinol Metab* 93:3215–3221.
- Nara N, et al. (2007) Disruption of CXC motif chemokine ligand-14 in mice ameliorates obesity-induced insulin resistance. *J Biol Chem* 282:30794–30803.
- Ferguson GJ, et al. (2007) PI(3)Kgamma has an important context-dependent role in neutrophil chemokinesis. *Nat Cell Biol* 9:86–91.
- Nishio M, et al. (2007) Control of cell polarity and motility by the PtdIns(3,4,5)P3 phosphatase SHIP1. *Nat Cell Biol* 9:36–44.
- Nugent C, Younossi ZM (2007) Evaluation and management of obesity-related nonalcoholic fatty liver disease. *Nat Clin Pract Gastroenterol Hepatol* 4:432–441.
- Rückle T, Schwarz MK, Rommel C (2006) PI3Kgamma inhibition: Towards an 'aspirin of the 21st century'? *Nat Rev Drug Discov* 5:903–918.
- Marone R, Cmilianovic V, Giese B, Wymann MP (2008) Targeting phosphoinositide 3-kinase: Moving towards therapy. *Biochim Biophys Acta* 1784:159–185.
- Chang JD, et al. (2007) Deletion of the phosphoinositide 3-kinase p110gamma gene attenuates murine atherosclerosis. *Proc Natl Acad Sci USA* 104:8077–8082.
- Kubota N, et al. (2008) Dynamic functional relay between insulin receptor substrate 1 and 2 in hepatic insulin signaling during fasting and feeding. *Cell Metab* 8:49–64.
- Ueki K, et al. (2002) Increased insulin sensitivity in mice lacking p85 β subunit of phosphoinositide 3-kinase. *Proc Natl Acad Sci USA* 99:419–424.
- Goyama S, et al. (2008) Evi-1 is a critical regulator for hematopoietic stem cells and transformed leukemic cells. *Cell Stem Cell* 3:207–220.
- Ito A, et al. (2008) Role of CC chemokine receptor 2 in bone marrow cells in the recruitment of macrophages into obese adipose tissue. *J Biol Chem* 283:35715–35723.

Adiponectin Enhances Insulin Sensitivity by Increasing Hepatic IRS-2 Expression via a Macrophage-Derived IL-6-Dependent Pathway

Motoharu Awazawa,¹ Kohjiro Ueki,^{1,2,*} Kazunori Inabe,¹ Toshimasa Yamauchi,¹ Naoto Kubota,^{1,2,3} Kazuma Kaneko,¹ Masatoshi Kobayashi,¹ Aya Iwane,¹ Takayoshi Sasako,¹ Yukiko Okazaki,¹ Mitsuru Ohsugi,¹ Iseki Takamoto,¹ Satoshi Yamashita,⁴ Hiroshi Asahara,⁴ Shizuo Akira,⁵ Masato Kasuga,⁶ and Takashi Kadowaki^{1,2,*}

¹Department of Diabetes and Metabolic Diseases, Graduate School of Medicine, University of Tokyo, Tokyo 113-8655, Japan

²Translational Systems Biology and Medicine Initiative (TSBMI), University of Tokyo, Tokyo 113-8655, Japan

³Clinical Nutrition Program, National Institute of Health and Nutrition, Tokyo 162-8636, Japan

⁴Department of Systems BioMedicine, National Research Institute of Child Health and Development, Tokyo 157-8535, Japan

⁵Laboratory of Host Defense, WPI Immunology Frontier Research Center, Osaka University, Osaka 565-0871, Japan

⁶Research Institute, International Medical Center of Japan, Tokyo 162-0052, Japan

*Correspondence: ueki-tky@umin.ac.jp (K.U.), kadowaki-3im@h.u-tokyo.ac.jp (T.K.)

DOI 10.1016/j.cmet.2011.02.010

SUMMARY

Insulin resistance is often associated with impeded insulin signaling due either to decreased concentrations or functional modifications of crucial signaling molecules including insulin receptor substrates (IRS) in the liver. Many actions of adiponectin, a well-recognized antidiabetic adipokine, are currently attributed to the activation of two critical molecules downstream of AdipoR1 and R2: AMP-activated kinase (AMPK) and peroxisome proliferator-activated receptor α (PPAR α). However, the direct effects of adiponectin on insulin signaling molecules remain poorly understood. We show here that adiponectin upregulates IRS-2 through activation of signal transducer and activator of transcription-3 (STAT3). Surprisingly, this activation is associated with IL-6 production from macrophages induced by adiponectin through NF κ B activation independent of its authentic receptors, AdipoR1 and AdipoR2. These data have unraveled an insulin-sensitizing action initiated by adiponectin leading to upregulation of hepatic IRS-2 via an IL-6 dependent pathway through a still unidentified adiponectin receptor.

INTRODUCTION

Insulin resistance is often caused by decreased levels of its critical signaling molecules, functional modifications of these proteins, or both (Hotamisligil et al., 1996; Taniguchi et al., 2006). IRS-1 and IRS-2 are abundant in liver and are essential regulators for glucose metabolism in physiological and pathological circumstances (Dong et al., 2006; Kubota et al., 2008; Sun et al., 1995; Tamemoto et al., 1994). IRS-2 expression is preferentially decreased in the livers of obese model mice (Shimomura et al., 2000), and disruption of hepatic IRS-2 leads to insulin resistance (Kubota et al., 2000), suggesting that

hepatic IRS-2 as well as IRS-1 is critical for the pathogenesis of systemic insulin resistance.

Adiponectin is an antidiabetic adipokine (Kadowaki et al., 2006), which enhances insulin action by several mechanisms, including suppression of gluconeogenesis and regulation of fatty acid metabolism (Awazawa et al., 2009; Berg et al., 2001; Yamauchi et al., 2001) as well as modulation of calcium signaling in skeletal muscles (Iwabu et al., 2010). To date, most of these actions have been attributed to the activation of two critical molecules downstream of AdipoR1 and AdipoR2, AMPK, and PPAR α (Iwabu et al., 2010; Yamauchi et al., 2002; Yamauchi et al., 2007). In obese model mice with insulin resistance, hypo-adiponectinemia (Yamauchi et al., 2001) often coexists with downregulation of hepatic insulin signaling; however, direct effects of adiponectin on insulin signaling molecules remain poorly investigated.

IL-6 is an inflammatory cytokine that has usually been related to insulin resistance, although some reports have paradoxically suggested that transient IL-6 upregulation contributes to improved insulin sensitivity (for a comprehensive review, see Pedersen and Febbraio, 2008). In contrast, adiponectin has been reported to exert anti-inflammatory actions (Huang et al., 2008), although it activates NF κ B and induces inflammatory cytokines in some contexts (Haugen and Drevon, 2007). It is not precisely understood how adiponectin is related to inflammatory responses and cytokine production, including that of IL-6.

In this report, we show that adiponectin upregulates the IRS-2 protein through activation of STAT3 associated with IL-6 production from macrophages, independently of its authentic receptors, AdipoR1 and AdipoR2. These data have unraveled a novel adiponectin biology including the existence of an unidentified receptor.

RESULTS

IRS-2 Expression Was Decreased in Livers of Adiponectin-Deficient Mice, and Adiponectin Administration Upregulated IRS-2 in Liver

To examine the direct effects of adiponectin on insulin signaling, we first investigated the expression of insulin signaling

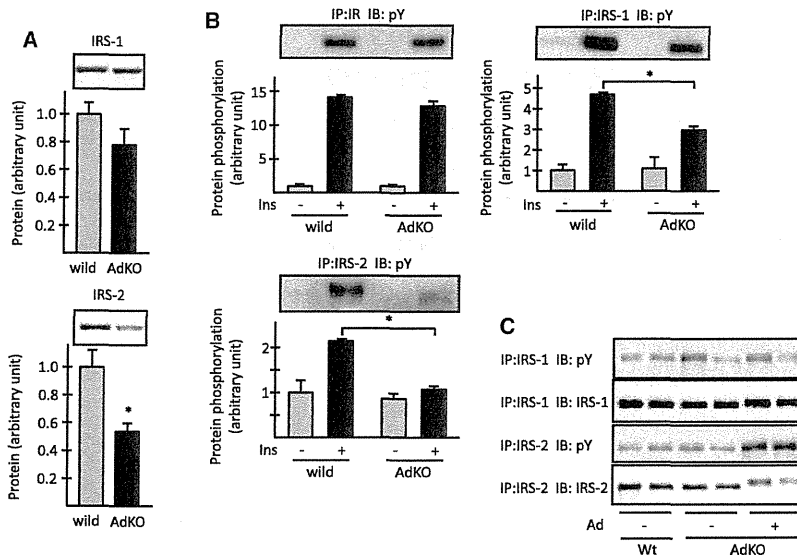


Figure 1. IRS-2 Expression Was Decreased in the Livers of Ad KO Mice

The representative blots of IRS-1 and IRS-2 in the livers of Ad KO mice and their arbitrary quantifications.

(A) Ad KO mice were sacrificed at the fasted state and the liver lysates were immunoprecipitated and immunoblotted with each antibody (n = 4, * p < 0.05).

(B) Ad KO mice were injected with insulin (Ins) and the livers were removed at 5 min. The lysates were immunoprecipitated with insulin receptor (IR), IRS-1, and IRS-2 antibody, respectively, and immunoblotted with 4G10 anti-phosphotyrosine (pY) antibody (n = 4, * p < 0.05).

(C) Ad KO mice were injected with adiponectin (Ad) intraperitoneally and the livers were removed at 4 hr. The lysates were immunoprecipitated with IRS-1 and IRS-2 antibody, respectively, and immunoblotted with pY, IRS-1 and IRS-2 antibody. Error bars represent mean \pm standard error of the mean (SEM).

molecules in the livers of adiponectin-deficient (AdKO) mice. The western blot revealed that IRS-2 protein levels were decreased in the livers of AdKO mice (Figure 1A), and IRS-2 phosphorylation by insulin was reduced (Figure 1B), while IRS-1 protein expression and its phosphorylation by insulin were relatively unaltered. Adiponectin administration in AdKO mice upregulated IRS-2 phosphorylation associated with its protein upregulation in liver (Figure 1C). These results prompted us to examine the possibility that adiponectin regulated IRS-2 expression in liver.

Adiponectin Upregulated IRS-2 and Restored Insulin Action in Livers of *db/db* Mice

We then administered adiponectin to *db/db* mice, an obese animal model with insulin resistance and selective downregulation of IRS-2 in the liver (Shimomura et al., 2000). Adiponectin administration, which raised the plasma concentration of adiponectin twice as high as preadministration levels (Figure S1A available online), restored hepatic IRS-2 protein and its phosphorylation (Figure 2A). This led to the recruitment of an adaptor molecule, the regulatory p85 subunit of phosphoinositide-3 (PI3) kinase, as assessed by the coimmunoprecipitation of IRS-2 and p85. In contrast, the expression and phosphorylation of insulin receptor (IR) and IRS-1 were unaltered with adiponectin administration (Figure 2A). Insulin stimulation after 4 hr of pretreatment with adiponectin showed partial but significant restoration of the impaired insulin signaling in livers of *db/db* mice, as evidenced by Akt and forkhead transcription factor FoxO1 phosphorylation, accompanied by IRS-2 upregulation (Figure 2B) and enhanced PI3 kinase activity associated with IRS-2 (Figure 2C), while IRS-1 phosphorylation and the PI-3 kinase activity associated with IRS-1 were unaltered. We also confirmed that adiponectin restored the downregulated IRS-2 and led to enhanced insulin signaling in high fat diet-induced obese mice (Figures S1B and S1C). These results indicated that adiponectin restored the attenu-

ated insulin actions in liver of obese model mice via IRS-2 upregulation.

Time course experiments showed that adiponectin robustly upregulated hepatic *Irs2* messenger RNA (mRNA) at 2 hr (Figure 2D) and transiently and maximally increased IRS-2 protein at 4 hr (data not shown). Importantly, adiponectin administration to *db/db* mice did not alter plasma glucose and insulin levels during 0.5–2 hr (data not shown), indicating that the changes in IRS-2 expression were the primary effects of adiponectin but not the consequence of altered plasma glucose or insulin levels, which could secondarily modulate IRS-2 expression. Moreover, adiponectin administration also increased IRS-2 protein in the livers of wild-type mice (Figure S1D).

The enhanced insulin signaling by adiponectin in the livers of *db/db* mice was associated with suppressed mRNA expressions of key gluconeogenic enzymes, phosphoenolpyruvate carboxykinase (*Pck1*) and glucose-6-phosphatase (*G6pc*) (Figure S1E) and led to lower plasma glucose concentrations in a pyruvate tolerance test (Figure S1F), suggesting that adiponectin administration suppressed gluconeogenesis in liver. In addition, adiponectin decreased the mRNA expression of sterol regulatory element binding protein 1c (*Srebp1c*). Hepatic de novo lipogenesis, as assessed by ^3H and ^{14}C incorporation into saponified triglyceride, also tended to be lower in adiponectin-treated *db/db* mice (Figure S1G and Figure S1H).

Adiponectin Activated STAT3 in Liver, which Was Associated with Elevated Plasma IL-6 Concentration

Previously, we identified AdipoR1 and R2 as the receptors for adiponectin, both of which are abundant in the liver (Yamauchi et al., 2003), while T-cadherin, another possible receptor for adiponectin, is abundant in the cardiovascular system (Hug et al., 2004). We therefore hypothesized that adiponectin regulated IRS-2 expression directly through AdipoR1 or R2 in the liver. However, knockdown of neither AdipoR1 nor R2 in the liver attenuated *Irs2* upregulation by adiponectin (Figures S2A and

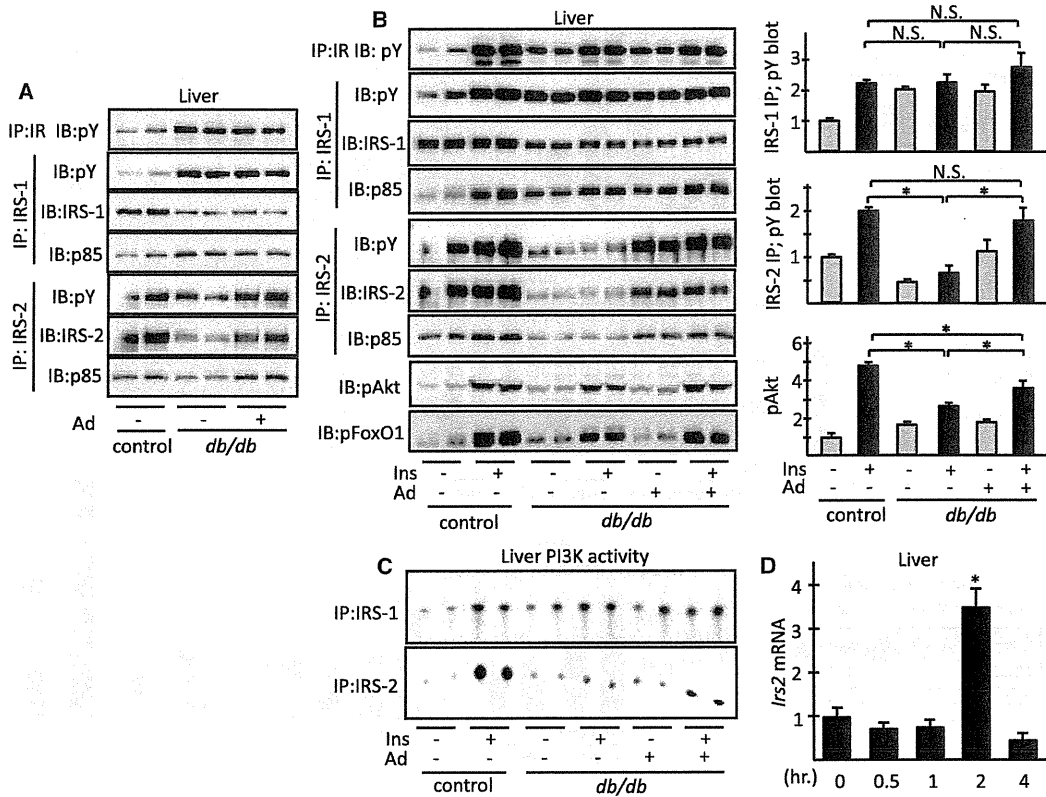


Figure 2. Adiponectin Upregulated IRS-2 Expression in the Liver of *db/db* Mice

(A–C) The representative blots of insulin signaling in the liver of *db/db* mice administered with adiponectin. (A) *db/db* mice and their control *misty/misty* mice were injected with adiponectin (Ad) at the fasted state, and the livers were removed at 4 hr. The lysates were immunoprecipitated with insulin receptor (IR), IRS-1, and IRS-2 antibody, respectively, and were subjected to immunoblotting with 4G10 anti-phosphotyrosine (pY), IRS-1, IRS-2, and p85 subunit of PI3Kinase (p85) antibody. (B) *db/db* mice and their control *misty/misty* mice were administered with Ad at the fasted state, and after 4 hr the mice were injected with insulin (Ins) via inferior vena cavae. The livers were removed at 5 min, except for phospho-FoxO1 blotting, for which the livers were removed at 2 min. The lysates were immunoprecipitated with IR, IRS-1, and IRS-2 antibody, respectively, and were subjected to immunoblotting with pY, IRS-1, IRS-2, p85, pAkt, and pFoxO1 antibody. The arbitrary quantifications are shown in the right-hand panels ($n = 6$, *; $p < 0.05$). (C) *db/db* mice and their control *misty/misty* mice were injected with Ad at the fasted state, and after 4 hr the mice were injected with insulin (Ins) via inferior vena cavae. The livers were removed at 2 min and subjected to PI3 kinase assay as described in the Experimental Procedures. (D) RT-PCR analysis of *Irs2* mRNA in the liver of *db/db* mice at indicated hours after Ad administration ($n = 4$, * $p < 0.05$). Error bars represent mean \pm SEM. See also Figure S1.

S2B). Furthermore, adiponectin stimulation did not upregulate *Irs2* in cultured hepatocytes (Figure S2C). These data raised the possibility that adiponectin indirectly upregulated hepatic IRS-2 through a previously unknown pathway.

To determine the mechanism of IRS-2 upregulation by adiponectin, we examined the changes in various signaling molecules in the liver after adiponectin administration, including those that had not been reported to regulate IRS-2. Of these, we noted strong phosphorylation of STAT3 in liver (Figure 3A). The time course in which the expression of the suppressor of cytokine signaling-3 (*Socs3*), the well-known downstream molecule of STAT3, was upregulated was almost identical with the time course in which *Irs2* was upregulated (Figure 3B), suggesting that *Irs2* and *Socs3* were upregulated by common upstream signaling(s). As expected, adiponectin stimulation of Fao cells

did not cause STAT3 phosphorylation (Figure 3C). From these data, we had an assumption that adiponectin induced some biological substances in the plasma, which then induced hepatic STAT3 phosphorylation and IRS-2 expression secondarily, although it had not been reported that STAT3 directly regulated IRS-2 expression.

Surprisingly indeed, we found that adiponectin administration caused an acute and transient increase of plasma IL-6, a potent activator of STAT3 (Figure 3D), the time course of which was coincident with the STAT3 phosphorylation in liver. *Il6* mRNA was strongly upregulated in white adipose tissue (WAT) after adiponectin administration, while the *Il6* mRNA in liver was also upregulated to a much lesser extent (Figure 3E, left panel). Further analysis revealed that *Il6* induction was more prominent in visceral WAT than in subcutaneous WAT, with the

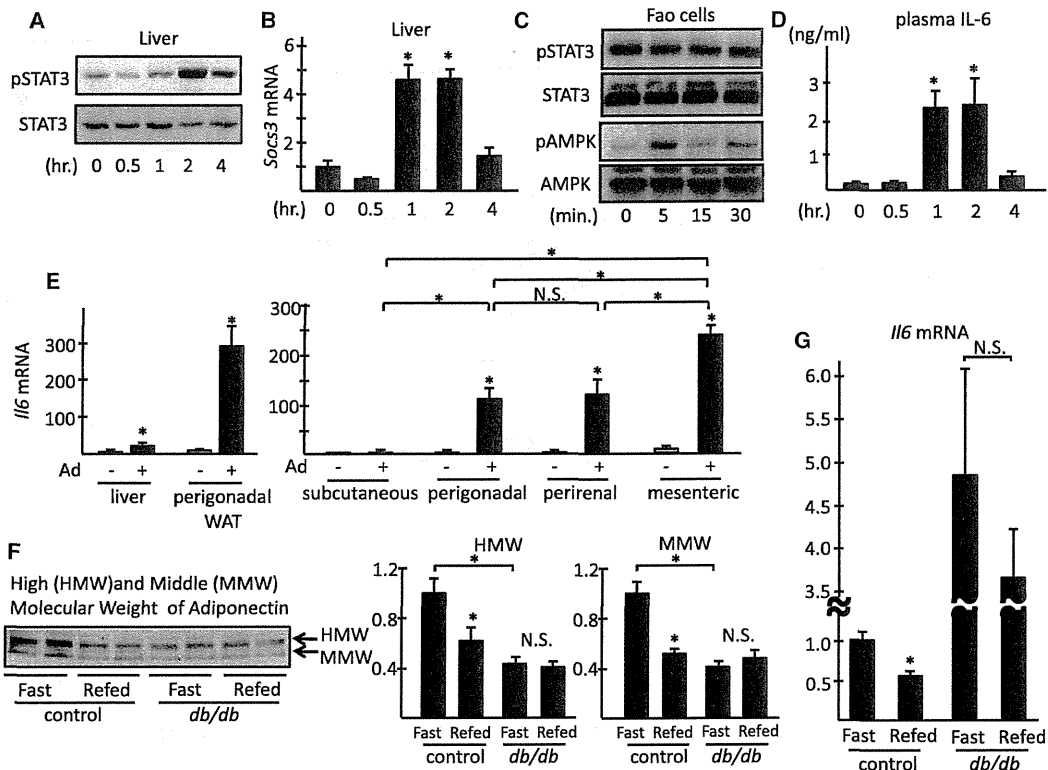


Figure 3. Hepatic STAT3 activation and IL-6 Induction after Adiponectin Administration

(A and B) The representative blot of pSTAT3/STAT3 (A) and RT-PCR analysis of *Socs3* mRNA (B) in the liver of *db/db* mice after adiponectin administration. *db/db* mice were injected with adiponectin (Ad) at the fasted state, and the livers were removed at the indicated hours. The lysates were immunoprecipitated with anti-STAT3 antibody and subjected to immunoblotting with pSTAT3 or STAT3 antibody. The total mRNA extracted from the livers was subjected to RT-PCR analysis ($n = 7-12$, $* p < 0.05$).

(C) The representative blots of pSTAT3/STAT3 and pAMPK/AMPK in Fao cells stimulated with Ad. Fao cells were stimulated with Ad at indicated time, and the lysates were immunoprecipitated with anti-STAT3 antibody and subjected to immunoblotting with pSTAT3 or STAT3 antibody. The total cell lysates were subjected to western blotting with pAMPK and AMPK antibody.

(D) The plasma IL-6 concentration after adiponectin administration. *db/db* mice were injected with Ad at the fasted state. The plasma collected at indicated hours was subjected to ELISA assay ($n = 7-12$, $* p < 0.05$).

(E) RT-PCR analysis of *I/6* mRNA in liver and various WAT depots. *db/db* mice were injected with Ad at the fasted state, and the livers and the adipose tissues were removed at 2 hr. The total mRNA was extracted and subjected to RT-PCR analysis ($n = 5-7$, $* p < 0.05$).

(F) The representative blot of the diurnal changes in plasma adiponectin concentrations and their arbitrary quantification. The blood samples of *db/db* and their control *misty/misty* mice collected at the fasted or refed state were subjected to immunoblotting with anti-adiponectin antibody ($n = 4$, $* p < 0.05$).

(G) The diurnal changes of *I/6* mRNA expression in perigonadal WAT. *db/db* and their control *misty/misty* mice were sacrificed at the fasted and refed state. The total mRNA was extracted from the perigonadal WAT and subjected to RT-PCR analysis ($n = 4-5$, $* p < 0.05$).

Error bars represent mean \pm SEM. See also Figure S2.

highest induction observed in mesenteric WAT (Figure 3E, right panel).

These data prompted us to hypothesize that adiponectin induced IL-6, which then activated hepatic STAT3 and subsequently upregulated IRS-2. Importantly, IRS-2 expression physiologically increases during fasting, and its function is crucial in the fasted state (Kubota et al., 2008). Indeed, consistent with our hypothesis, *I/6* expression was upregulated in the fasted state in WAT of wild-type mice and was associated with increased plasma adiponectin levels (Figures 3F and 3G). In contrast, *I/6* expression was highly and persistently upregulated in *db/db* mice with continuous downregulation of plasma adiponectin levels, regardless of the feeding state (Figures 3F and 3G).

IRS-2 Upregulation by Adiponectin was Mediated by Hepatic STAT3 Activation via IL-6

To verify our hypothesis, we first abrogated IL-6 action either by using neutralizing antibody or through genetic ablation (IL-6 knockout [KO] mice). Antibody-mediated IL-6 neutralization significantly attenuated hepatic STAT3 phosphorylation by adiponectin and abrogated the adiponectin-induced *Irs2* upregulation despite robust *I/6* induction (Figure 4A), which was confirmed by mRNA expression in perigonadal WAT. Moreover, in IL-6 KO mice, adiponectin-induced STAT3 phosphorylation and *Irs2* upregulation were totally abolished (Figure 4B).

In contrast, IL-6 administration upregulated *Irs2* mRNA and its phosphorylation in liver (Figure 4C) after phosphorylation of

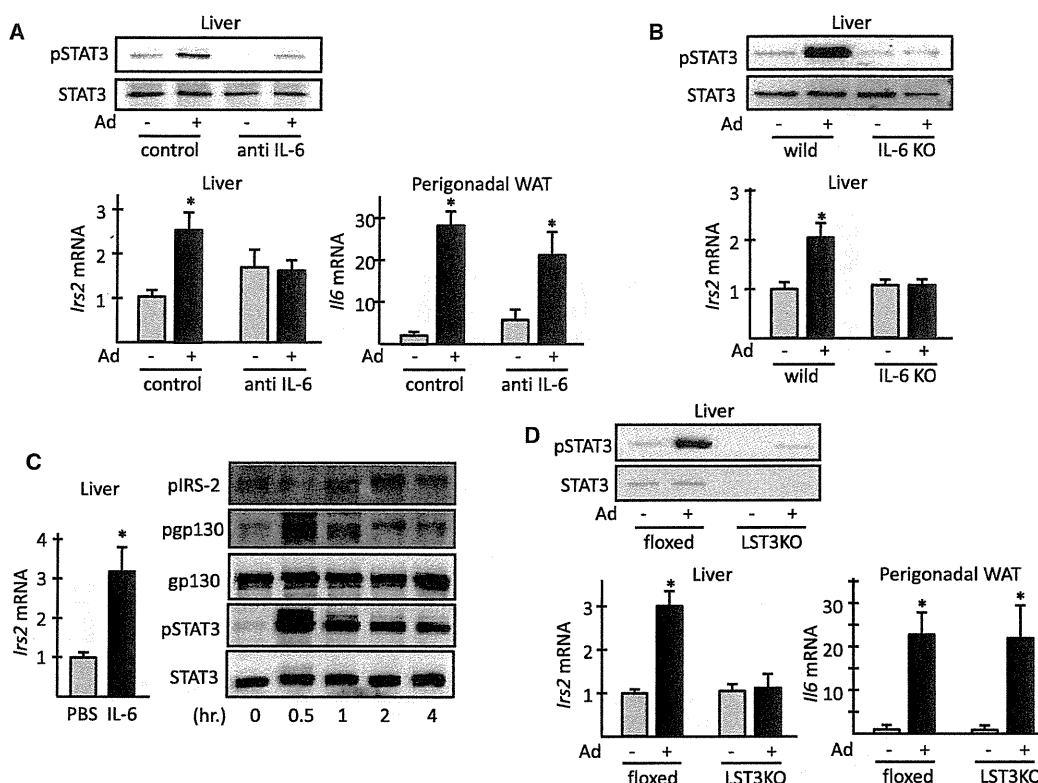


Figure 4. IL-6/STAT3 Signaling and Hepatic IRS-2 Upregulation by Adiponectin

(A) STAT3 signaling and IRS-2 induction with anti-IL6 antibody pretreatment. C57BL/6J mice pretreated with anti-IL6 antibody as described in the Experimental Procedures were injected with adiponectin (Ad) intraperitoneally, and the livers and perigonadal WAT were removed at 2 hr. The lysates of the livers were subjected to immunoblotting with pSTAT3/STAT3 antibody. The total mRNA was subjected to RT-PCR analysis for *Irs2* expression in liver and *I/6* expression in perigonadal WAT (n = 5, * p < 0.05).

(B) STAT3 signaling and IRS-2 induction in IL-6 KO mice. IL-6KO mice and their control C57BL/6J (wild) mice were injected with Ad intraperitoneally, and the livers were removed at 2 hr. The lysates of the livers were subjected to immunoblotting with pSTAT3/STAT3 antibody. The total mRNA was subjected to RT-PCR analysis for *Irs2* expression in liver (n = 5, * p < 0.05).

(C) STAT3 signaling and IRS-2 expression in liver after IL-6 administration. C57BL/6J mice were injected with recombinant human IL-6 intraperitoneally. The livers were removed at the indicated hours. The total mRNA extracted from the liver at 1 hr after IL-6 administration was subjected to RT-PCR analysis. The lysates of each liver sample were subjected to immunoprecipitation with the antibody for IRS-2, gp130, and STAT3, respectively, and subjected to immunoblotting with 4G10 anti-phosphotyrosine (for pIRS-2 and pgp130), gp130, pSTAT3, and STAT3 antibody as indicated (n = 5-6, * p < 0.05).

(D) STAT3 signaling and IRS-2 induction in LST3KO. LST3KO or their control *flax/flax* mice (floxed) were injected with Ad intraperitoneally, and the livers and perigonadal WAT were removed at 2 hr. The lysates of the livers were subjected to immunoblotting with pSTAT3/STAT3 antibody. The total mRNA was subjected to RT-PCR analysis for *Irs2* expression in liver and *I/6* expression in perigonadal WAT (n = 4-6, * p < 0.05).

Error bars represent mean ± SEM.

STAT3 and gp130 at 0.5 hr. The maximal *Irs2* mRNA upregulation after IL-6 administration occurred at 0.5–1 hr (data not shown), whereas the maximal STAT3 phosphorylation and *Irs2* upregulation after adiponectin administration occurred at 2 hr, further supporting that adiponectin secondarily upregulated IRS-2 via IL-6 induction.

Next, we administered adiponectin to mice with targeted disruption of STAT3 specifically in hepatocytes (LST3KO). In the livers of LST3KO mice, adiponectin-induced STAT3 phosphorylation and *Irs2* upregulation were totally abolished, while *I/6* induction by adiponectin was similar to that seen in the control *flax/flax* mice (Figure 4D). Collectively, these data indicated that adiponectin upregulated IRS-2 through STAT3 activation in hepatocytes in an IL-6-dependent manner.

Adiponectin-Induced IRS-2 Upregulation Was Mediated by STAT3 Recruitment to *Irs2* Promoter in Hepatocytes

Next, we focused on IRS-2 regulation by STAT3. Adenoviral-mediated overexpression of a constitutively active form of STAT3 (CA-STAT3) significantly increased IRS-2 in Fao cells (Figure 5A). Luciferase assay showed that wild-type (WT) or CA-STAT3 overexpression robustly enhanced *Irs2* promoter activity of the –1300 bps region, while the induction was diminished in the promoter deleted up to –500 bps (Figure 5B). The promoter region from –500 to –1300 bps contains multiple potential STAT3 binding sites. Indeed, chromatin immunoprecipitation (ChIP) assay in vivo confirmed that immunoprecipitation with STAT3 antibody significantly enriched the *Irs2* promoter regions in the livers at 1 and 2 hr after adiponectin administration,

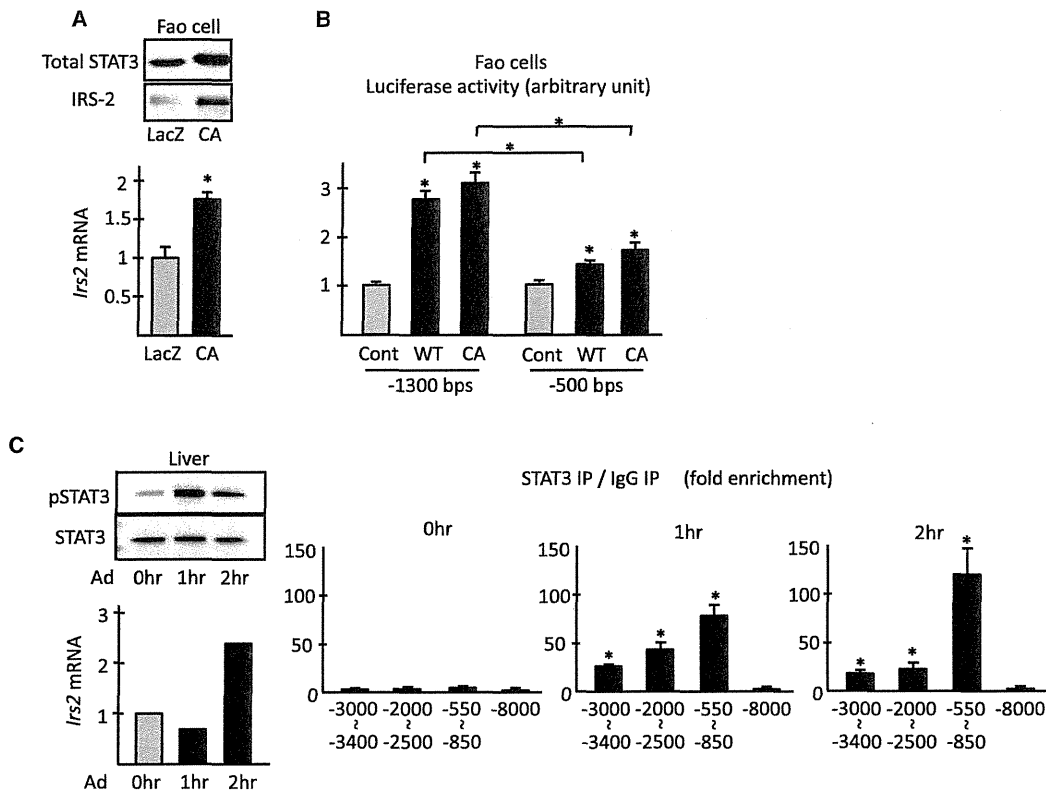


Figure 5. STAT3 Involvement in Hepatic IRS-2 Upregulation by Adiponectin

(A) Fao cells were infected with adenovirus encoding constitutively active STAT3 (CA) or LacZ. At 48 hr after infection, the cells were subjected to immunoprecipitation and immunoblotting with STAT3 and IRS-2 antibody, respectively. The total mRNA was subjected to RT-PCR analysis ($n = 4$, $* p < 0.05$). (B) *Irs2* promoter activity in Fao cells. Fao cells transfected with the reporter vector harboring -1300 or -500 bp *Irs2* promoter were overexpressed with wild-type (WT) or CA STAT3. The cells were subjected to luciferase assay. The arbitrary units of luciferase activity are shown ($n = 4$, $* p < 0.05$). (C) Chromatin immunoprecipitation of *Irs2* promoter regions with STAT3 antibody in liver. *db/db* mice were injected with adiponectin (Ad) at the fasted state, and the livers were removed at the indicated hours. The western blot of pSTAT3 and the mRNA expression of *Irs2* are shown in the left panels. The livers were immunoprecipitated with anti-STAT3 antibody, and -3000 to -3400 , -2000 to -2500 , and -550 to -850 of *Irs2* promoter region in the immunoprecipitated DNA was quantified by RT-PCR analysis. Fold enrichment compared to immunoprecipitation with control IgG antibody is shown ($n = 3$, $* p < 0.05$). Error bars represent mean \pm SEM.

with the -550 to -850 regions showing the highest enrichment (Figure 5C).

Adiponectin Induced IL-6 from Macrophages

We next investigated the origin of IL-6 induction by adiponectin. Fractionation experiments of the perigonadal WAT of adiponectin-treated *db/db* mice revealed that *Il6* mRNA was almost exclusively detected in the stromal vascular cell (SVC) fraction (Figure 6A). This finding was consistent with the immunohistochemistry analyses showing that IL-6 was exclusively contained with F4/80 in perigonadal WAT of adiponectin-treated *db/db* mice (Figure 6B). Indeed, adiponectin strongly upregulated *Il6* expression in cultured macrophages such as RAW264.7 cells or primary peritoneal macrophages, and not in fully differentiated 3T3L1 adipocytes (Figure 6C). We also conducted bone marrow transplantation (BMT) experiments, in which IL-6 KO mice were transplanted with BM from either IL-6 KO mice or wild-type mice. At 8 weeks after BMT, $>99\%$ of the leukocytes in peripheral blood were repopulated by donor cells (data not shown). IL-6

KO mice with the wild-type BM showed robust IL-6 induction by adiponectin and displayed significant *Irs2* upregulation in liver (Figure 6D), indicating that the IL-6 from BM-derived mononuclear cells was sufficient for IRS-2 induction by adiponectin. Importantly, adiponectin stimulation did not induce *Il6* in Fao cells (data not shown), indicating that the weak *Il6* mRNA induction observed in the livers of *db/db* mice or IL-6 KO mice transplanted with wild-type BM could be accounted for by non-hepatocyte cells, such as Kupffer cells or the resident macrophages in liver.

Adiponectin Induced IL-6 via NF κ B Pathway in a Form-Dependent Manner, Independently of AdipoR1/AdipoR2

We further investigated the mechanism of IL-6 induction by adiponectin. Adiponectin-induced IL-6 production was associated with a decrease of I κ B α , the inhibitory molecule of NF κ B, in perigonadal WAT (Figure 7A). Indeed, ChIP assay with mouse peritoneal macrophages showed that immunoprecipitation with NF κ B

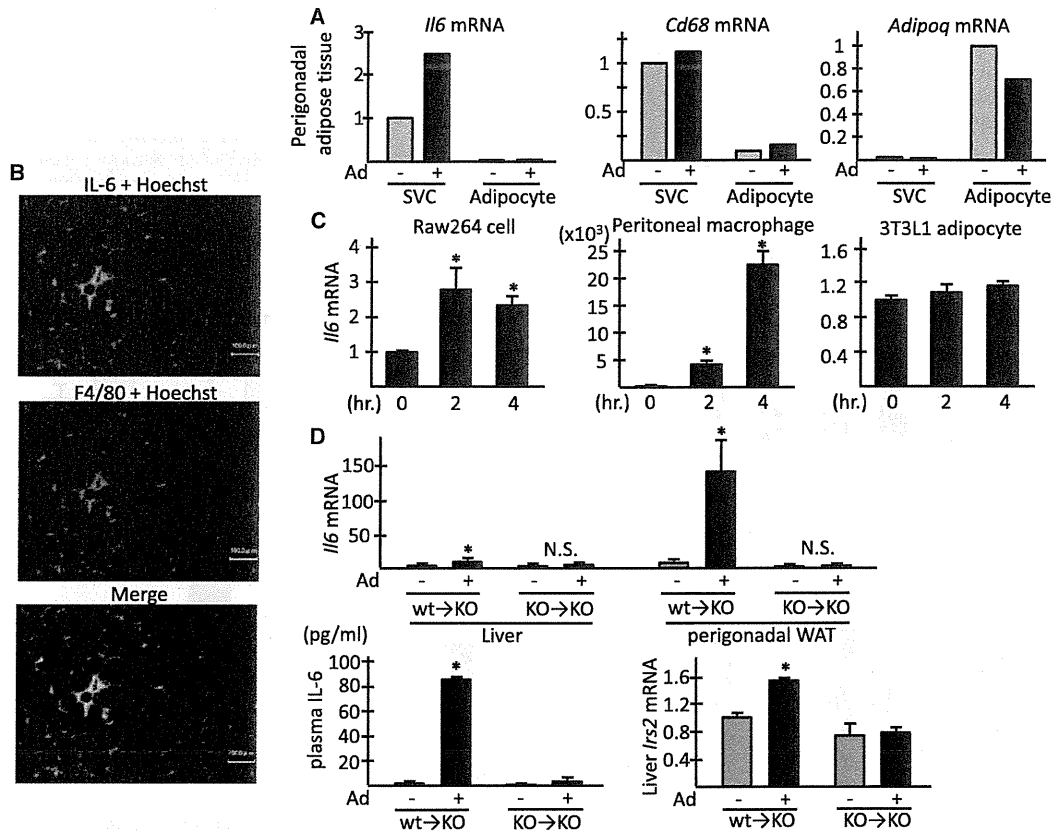


Figure 6. Upregulation of IL-6 by Adiponectin from Macrophages

(A) *Il6* expression in stromal vascular cells (SVCs) and adipocytes from perigonadal WAT of *db/db* mice injected with adiponectin. The *db/db* mice were injected with adiponectin (Ad) at the fasted state, and the perigonadal WAT was removed at 2 hr. SVCs and adipocytes were fractionated and subjected to mRNA extraction and RT-PCR analysis.

(B) IL-6 staining of perigonadal WAT after adiponectin administration. *db/db* mice were injected with Ad at the fasted state, and the perigonadal WAT was removed at 2 hr. The samples were subjected to immunostaining for F4/80 (red), IL-6 (green), and DNA (blue).

(C) RT-PCR analysis for *Il6* mRNA expression in RAW264.7 cells, primary peritoneal macrophages and fully differentiated 3T3L1 adipocytes after Ad stimulation (n = 5, * p < 0.05).

(D) IL-6 induction and IRS-2 upregulation in IL-6 KO mice transplanted with bone marrow from wild-type C57BL/6J mice. The IL-6 KO mice transplanted with bone marrow from wild-type C57BL/6J mice (wt → KO) or IL-6 KO mice (KO → KO) were injected with Ad at the fasted state. The plasma was collected, and the liver and the perigonadal adipose tissues were removed at 2 hr. Plasma IL-6 concentration was determined by ELISA assay, and the total mRNA from the tissues was subjected to RT-PCR analysis (n = 5–6, * p < 0.05). Error bars represent mean ± SEM.

p65 subunit antibody significantly enriched the NFκB binding site of *Il6* promoter region (Liebermann and Baltimore, 1990) after adiponectin stimulation (Figure 7B), suggesting that adiponectin induced IL-6 in macrophages through transcriptional regulation by NFκB.

Adiponectin exists in various forms in plasma such as trimer, hexamer, and high molecular weight (HMW), as well as a proteolytically cleaved form, globular adiponectin (Fruebis et al., 2001; Waki et al., 2005). It has been reported that the globular, trimer, and higher-molecular-weight forms of adiponectin activate AMPK via AdipoR1, whereas the HMW form also activates NFκB (Tsao et al., 2003). As nonreduced PAGE showed that the full-length adiponectin that we prepared contained trimer, hexamer, and higher-molecular-weight complexes (data not shown), it was unclear which form of adiponectin was respon-

sible for IL-6 production in our study. In addition, adiponectin, which we prepared from *E. coli*, was inevitably contaminated with lipopolysaccharide (LPS), a strong inducer of IL-6 production, although the degree of LPS was as low as 1 pg/mg adiponectin after meticulous decontamination (data not shown). To address these issues, we stimulated RAW264.7 cells with various forms of adiponectin prepared from mammalian cells or *E. coli*. The results showed that the full-length adiponectin was the most potent, and the trimeric form was a less potent inducer of IL-6, whereas globular adiponectin did not induce IL-6 at all (Figure 7C). The form dependency was irrelevant to whether adiponectin was prepared from mammalian cells or *E. coli*.

Even more intriguingly, disruption of AdipoR1 and AdipoR2 (DKO) (Yamauchi et al., 2007) still showed robust upregulation

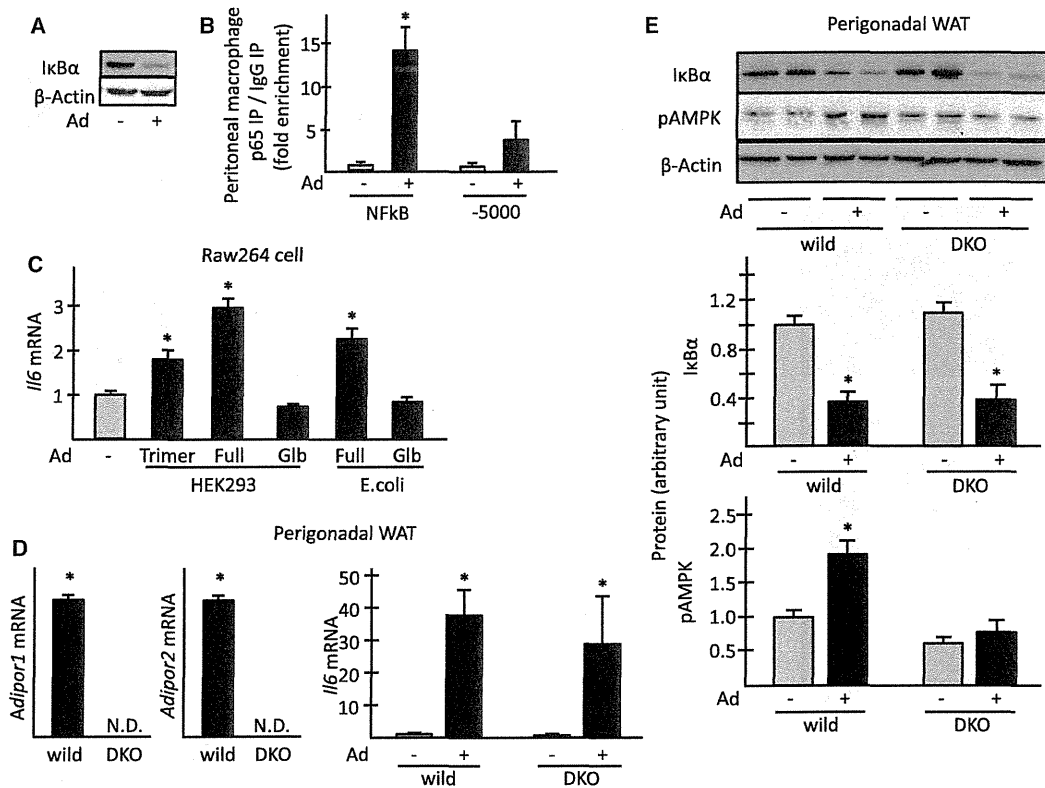


Figure 7. Upregulation of IL-6 via NFκB Pathway by Adiponectin in a Form-Dependent Manner Independently of Adiponectin Receptors (A and B) Activation of NFκB pathway by adiponectin.
 (A) The *db/db* mice were injected with adiponectin (Ad) at the fasted state, and the perigonadal WAT was removed at 2 hr. The total cell lysates were subjected to western blotting with the antibody for IκBα or β-actin.
 (B) Chromatin immunoprecipitation of *Il6* promoter with the antibody for p65 subunit of NFκB. The mouse primary peritoneal macrophages were stimulated with Ad for 2 hr. The cells were immunoprecipitated with p65 antibody, and the precipitated DNA of NFκB binding site of *Il6* promoter was quantified by RT-PCR analysis. The -5000 region of the *Il6* promoter was used as the negative control. Fold enrichment compared to immunoprecipitation with control IgG antibody is shown (n = 3, *; p < 0.05).
 (C) RT-PCR analysis of *Il6* mRNA in RAW264.7 cells stimulated with various forms of adiponectin (Ad). RAW264.7 cells were stimulated with 25 μg/ml trimeric form (Trimer), full-length (Full), or globular form (Glob) adiponectin prepared from HEK293 or *E. coli* for 2 hr. The total mRNA was subjected to RT-PCR analysis. (n = 4, * p < 0.05).
 (D and E) IL-6 induction and IκBα degradation in perigonadal adipose tissues of AdipoR KO mice. The mice with targeted disruption of AdipoR1 and AdipoR2 (DKO) or their control mice were injected with Ad at the fasted state. The perigonadal WAT was removed at 2 hr and the total mRNA was subjected to RT-PCR analysis for *Adipor1*, *Adipor2* and *Il6* expression (n = 5, * p < 0.05; N.D., not detected) (D) or the total cell lysates were immunoblotted with IκBα, pAMPK and β-actin antibody (E). The arbitrary quantifications of immunoblots were shown in the lower panel (n = 3–5, * p < 0.05). Error bars represent mean ± SEM. See also Figure S3.

of *Il6* by adiponectin in the perigonadal WAT (Figure 7D). The degradation of IκBα by adiponectin was also observed, while AMPK activation, the downstream molecule of AdipoR1, was abrogated (Figure 7E). As T-cadherin (*Cdh13*) mRNA was undetectable in RAW264.7 cells (data not shown), consistent with the previous report (Ivanov et al., 2001), these data suggest that there still exists an unidentified molecule in macrophages functioning as the receptor for hexamer or HMW adiponectin that mediates IL-6 upregulation.

DISCUSSION

In this study, we have discovered a pathway in which adiponectin upregulates IRS-2 in liver. The data also suggest the exist-

tence of an unidentified adiponectin receptor and indicate that the activation of STAT3 and subsequent increase in IRS-2 are mediated by IL-6 (Figure S3).

As previously reported, adiponectin activates AMPK, which suppresses gluconeogenic gene expressions (Yamauchi et al., 2002). Here, we propose that the IRS-2-mediated insulin-sensitization could be, besides AMPK activation, another mechanism whereby adiponectin exerts its antidiabetic actions. IRS-2 upregulation by adiponectin suppresses gluconeogenesis but does not enhance lipogenesis, consistent with our previous report showing that the suppression of SREBP1c is mediated largely via AMPK (Awazawa et al., 2009) and that IRS-2 mainly contributes to suppression of gluconeogenesis by insulin (Kubota et al., 2008).

IRS-1 and IRS-2 have partially overlapping but distinct functions in liver. Especially during the fasted state, IRS-2 increases and plays pivotal roles at its peak level immediately after refeeding (Kubota et al., 2008), while IRS-1 dominates during refeeding or in refed conditions (Guo et al., 2009). To date, several pathways have been identified to regulate IRS-2 expression, such as cAMP response element binding protein (CREB) and FoxO1 during fasting (Ide et al., 2004; Jhala et al., 2003; Shimomura et al., 2000) and SREBP1c after refeeding (Ide et al., 2004). Our findings suggest a mechanism of IRS-2 regulation via STAT3.

IL-6 activates STAT3 via IL-6 receptor/gp130 complex, while STAT3 is known to be phosphorylated by other cytokines (Levy and Darnell, 2002). Previous reports have suggested that the activation of gp130 interfacing with receptors other than the IL-6 receptor also contributes to STAT3 activation by IL-6 (Ernst et al., 2001). In our experiment, STAT3 phosphorylation reached its peak at 0.5–1 hr after IL-6 administration, whereas plasma IL-6 elevation and the maximal STAT3 phosphorylation concurrently occurred at 1–2 hr after adiponectin administration. Comparing the time course of these suggests that STAT3 activation induced by adiponectin is via the direct binding of IL-6 to the IL-6/gp130 receptor, although the possibility still remains that other ligand-receptor interactions are also involved.

Although IL-6 has usually been related to insulin resistance (Pradhan et al., 2001), some reports have paradoxically suggested that IL-6 contributes to improved insulin sensitivity (reviewed in Pedersen and Febbraio, 2008). Our data indicate that transient elevation of IL-6 levels leads to IRS-2 upregulation and enhances insulin signaling in liver. In contrast, in obese model mice, hepatic IRS-2 is downregulated in liver in spite of chronic plasma IL-6 elevation, possibly due to hyperinsulinemia. Even under these pathological conditions, the transient further increase in IL-6 levels accomplished by therapeutic administration of adiponectin leads to STAT3 phosphorylation and IRS-2 upregulation, suggesting that the acute change in IL-6 level, regardless of its absolute value, is critical for the subsequent STAT3 activation and IRS-2 upregulation. Indeed, transient IL-6 upregulation occurs in some physiologic circumstances such as muscle contraction, which is implicated in insulin sensitivity (Febbraio et al., 2004; Kelly et al., 2009). We have also found that in physiologic conditions IL-6 and adiponectin show similar diurnal variation in their expressions with their peaks in the fasting state, although the causal relations between these circadian changes and their physiological implications are not fully tested and need to be further validated. There is also still much debate as to whether chronically elevated IL-6 levels could actually contribute to systemic insulin resistance in obesity (Holmes et al., 2008; Torisu et al., 2007); this concept awaits future research.

We have shown by *in vitro* and BMT experiments that the macrophages mediate, and are sufficient for, the IL-6 induction and the resultant IRS-2 upregulation by adiponectin. Whereas IL-6 is known to be produced in adipocytes (Fain et al., 2004; Kershaw and Flier, 2004), our results consistently indicate that the IL-6 is mainly derived from SVCs, although the experiment using isolated SVCs could have a limitation due to the strong induction of IL-6 during the isolation process (Ruan et al., 2003). However, our data indicate that the *Il6* induction in liver by adiponectin originated in non-hepatocyte cells such as

Kupffer cells, consistent with our previous report showing that AdipoR1/2 are the only functional receptors in hepatocytes (Yamauchi et al., 2007). We hypothesize that the unknown adiponectin receptor suggested here, which mediates *Il6* induction via the NF κ B pathway, is expressed in macrophages but not in hepatocytes or adipocytes. This hypothesis explains the strong and specific IL-6 production in macrophages induced by adiponectin, although we could not completely rule out the possibility that other cells or tissues also contribute to IL-6 induction by adiponectin. The identification of the still unknown receptor in the future will resolve this issue and will also add depth to our knowledge about the field of metabolism by clarifying the significance of IRS-2 regulation as well as IL-6 induction by adiponectin in physiological or pathophysiological settings.

Previous reports indicate that adiponectin suppresses inflammatory responses induced by hyperglycemia (Devaraj et al., 2008) or TNF- α (Zhang et al., 2009), while others have reported that adiponectin by itself activates NF κ B and promotes inflammatory cytokine production (Haugen and Drevon, 2007; Rovin and Song, 2006). The important aspect of this issue is that adiponectin could exert diverse effects upon inflammation and metabolism through different pathways. AMPK, as an anti-inflammatory molecule, is activated by various forms of adiponectin (Tsao et al., 2002), presumably via AdipoR1, while NF κ B has been shown to be activated by the HMW form (Tsao et al., 2003). As we have shown here, IL-6 is upregulated by adiponectin, whereas AMPK activation is totally abolished, in AdipoR1 and R2 knockout mice. T-cadherin, another possible receptor for hexameric and HMW forms of adiponectin in the cardiovascular system (Denzel et al., 2010; Hug et al., 2004), is undetectable in macrophages *in vivo* (Ivanov et al., 2001) and in RAW264.7 cells in our own study. These data indicate that there still exists an unidentified molecule in macrophages functioning as the receptor for hexamer or HMW adiponectin, and that adiponectin could exert distinct actions through different receptors in a context-dependent manner.

In conclusion, we have unraveled an insulin-sensitizing action initiated by adiponectin leading to upregulation of hepatic IRS-2 via a macrophage-derived IL-6-dependent pathway. Our data not only provide insight into adiponectin biology including the existence of a still unidentified adiponectin receptor, but also challenge the widely accepted idea about how IL-6/STAT3 signaling serves for systemic glucose metabolism, suggesting the possibility that recovery or creation of diurnal variations of adiponectin/IL-6 axis can be a therapeutic strategy for obesity-induced insulin resistance.

EXPERIMENTAL PROCEDURES

Reagents

Recombinant adiponectin was prepared as described previously (Yamauchi et al., 2002). Trimeric and full-length forms of adiponectin derived from HEK293 cells, and globular adiponectin derived from *E. coli* were purchased from ProSpec. Globular adiponectin derived from HEK293 cells was purchased from Alexis Biochemicals. Recombinant human IL-6 was purchased from R&D systems.

Animals

BKS.Cg-*m* ^{+/+} *Lep^{db}*/*J* (*db/db*) mice and C57BL/6J mice were purchased from Japan CLEA. C57BL/6J.129S6-*Il6^{tm1Kopf}* (IL-6 KO) mice were purchased

from Jackson laboratory. Generation of Ad KO mice and AdipoR-deficient mice were described previously (Kubota et al., 2002; Yamauchi et al., 2007). LST3KO mice were kindly provided by H. Inoue and M. Kasuga (Inoue et al., 2004). The mice were injected with 3 μ g/g BW recombinant adiponectin intraperitoneally after overnight fasting at the age between 8 and 10 weeks. A total of 1 μ g/g BW recombinant human IL-6 was injected to C57BL/6J mice (Cressman et al., 1996; Yamada et al., 1997). For western blotting, five units of insulin was injected into the inferior vena cavae of anesthetized mice, and the livers were removed after 5 min, except for western blotting of phospho-FoxO1, where the livers were removed after 2 min. The Animal Care Committee of the University of Tokyo approved the animal care and experimental procedures.

Immunoprecipitation and Immunoblotting

Immunoprecipitation and immunoblotting were conducted as previously described (Awazawa et al., 2009). The blood samples were collected from the mice after 24 hr fasting or 4 hr refeeding, and 1 μ l plasma was subjected to adiponectin immunoblotting. 4G10, anti-IRS-1, anti-IRS-2, and anti-PI3-K p85 subunit N-SH2 antibodies were purchased from Millipore. Anti-insulin receptor antibody (C-19) and anti-gp130 antibody (C-20) were purchased from SantaCruz Biotechnology. Antibody for the p65 subunit of NF κ B (ab7970) and adiponectin were purchased from Abcam. All the other antibodies were purchased from Cell Signaling Technology.

PI3 Kinase Assay

Five units of insulin was injected into the inferior vena cavae of anesthetized mice, and the livers were removed after 2 min. PI3 kinase activities in the liver was determined in immunoprecipitates with the indicated antibodies as previously described (Ueki et al., 2000). The phosphorylated lipids were visualized by autoradiography with an image analyzer (BAS 2000; Fuji Film, Tokyo).

Quantitative Real-Time PCR

The total RNA was prepared by RNeasy kit (QIAGEN). Complementary DNA was prepared by Reverse Transcription Reagents (Applied Biosystems). Quantitative real-time PCR was performed with ABI Prism with PCR Master Mix Reagent (Applied Biosystems) except for quantification of *Irf6* mRNA in BMT experiment, where Power SYBR Green PCR Master Mix was used with the primers as follows: fwd, TTCCATCCAGTTGCCCTTCTTG; rev, TTCTCATTTCCAGATTCCAG. Levels of mRNA were normalized to that of cyclophilin (Awazawa et al., 2009). The other primers and probes were purchased from Applied Biosystems.

Cells and Cell Culture

RAW264.7 cells and fully differentiated 3T3L1 cells were cultured in DMEM (GIBCO) medium. Fao cells were cultured in RPMI1640 (GIBCO) medium. Primary peritoneal macrophages were isolated from 8-week-old male C57BL/6J mice injected with 3% thioglycollate. Isolation of adipocytes and SVCs was conducted as previously described (Kamei et al., 2006). All the media were supplemented with 10% (vol/vol) fetal bovine serum (GIBCO). Where indicated, the cells were infected with adenoviruses and harvested 48 hr after infection, and cells were stimulated with 25 μ g/ml adiponectin.

Generation and Infection of Adenoviruses

Adenovirus of a constitutively active form of STAT3 was kindly provided by H. Inoue and M. Kasuga (Kobe University) (Inoue et al., 2004). Prior to use, all adenoviruses were purified on a cesium chloride gradient and dialyzed into PBS plus 10% glycerol. The cells were infected with the adenoviruses at the MOI (multiplicity of infection, or number of viral particles per cell) of 1000 PFU/cell.

IL-6 Neutralization

C57BL/6J mice were injected with 47 μ g of anti-IL6 antibody or its isotype control (R&D Systems) via tail vein. The following day after overnight fasting, the mice were injected with 3 μ g/g BW recombinant adiponectin intraperitoneally and sacrificed at 2 hr.

Luciferase Assay

Luciferase reporter plasmid harboring 5'-flanking region of mouse *Irs2* exon 1 was subcloned to pGL3 basic vector. Fao cells plated onto a 24-well plate were transfected with 0.5 μ g of each luciferase reporter plasmid and 0.02 μ g *Renilla* luciferase plasmid with HSV-TK promoter (pRL-TK, Promega) with Lipofectamine 2000 (Invitrogen). On the fourth day, the cells were harvested and the luciferase activity was measured by Dual-Luciferase Reporter Assay System (Promega) according to the manufacturer's protocol.

Chromatin Immunoprecipitation Assay

ChIP assay was conducted as previously described (Friedman et al., 2004). In brief, mouse peritoneal macrophages or 1 g mouse liver was crosslinked in 1% formaldehyde/PBS. The tissue was suspended in lysis buffer (50 mM Tris-HCl [pH 8.1], 10 mM EDTA, 1% SDS, and protease inhibitor) and the chromatin was sheared by Bronson Sonifier 250D. The lysates were diluted five times with dilution buffer (16.7 mM Tris-HCl [pH 8.1], 167 mM NaCl, 1.2 mM EDTA, 0.01% SDS, 1.1% Triton X-100, and protease inhibitor). The chromatin solution was incubated with 2 μ g primary antibodies and Dynabeads Protein A (Invitrogen). The beads were rinsed with wash buffer (50 mM HEPES-KOH [pH 7.0], 0.5 M LiCl, 1 mM EDTA, 0.7% sodium deoxycholate, and 1% NP-40) and immune complexes were eluted from beads with elution buffer (50 mM Tris-HCl [pH 8.0], 10 mM EDTA, 1% SDS) at 65°C. Eluates were additionally incubated at 65°C to reverse crosslinking and then incubated with 0.5 mg/ml Proteinase K at 55°C. DNA was purified with MinElute PCR purification kit (QIAGEN). The immunoprecipitated DNA regions were quantified by real time PCR using ABI Prism. (See also Table S1.)

Immunohistochemistry

The perigonadal fat pads were fixed in 4% paraformaldehyde in PBS and embedded in paraffin. The sections were incubated with rat F4/80 antibody (Serotec) (1:250 dilution) and goat IL-6 antibody (Santa Cruz) (1:50 dilution) at 4°C, followed by incubation with anti-rat IgG RITC (Santa Cruz) and anti-goat IgG FITC (Santa Cruz) for 1 hr at room temperature. Hoechst staining (1:400 dilution) was performed for 20 min at room temperature. The sections were mounted with Fluorescent Mounting Medium (DAKO) and examined under a fluorescence microscope (BZ-8000) (KEYENCE).

Analytical Procedures

Blood samples were collected by tail bleed. Plasma adiponectin and IL-6 concentrations were quantified by ELISA assay (Ohtuka Pharmaceuticals and R&D Systems, respectively).

Bone Marrow Transplantation

Bone marrow cells were collected by flushing of the femurs and tibiae of the mice at 6 weeks of age. The nucleated cells were counted and injected intravenously into lethally irradiated (10 Gy) male IL-6 KO mice at 6 weeks of age. The mice were maintained under normal chow diet for 8 weeks before experiments. For chimerism assay, the genomic DNA purified from the blood samples was subjected to Real-time PCR as previously described (Ichikawa et al., 2008).

Statistical Analysis

Statistical analysis was performed by two-sample t test assuming unequal variances or paired two-sample t test for means. Statistical significance was accepted at $p < 0.05$ unless otherwise indicated.

SUPPLEMENTAL INFORMATION

Supplemental Information includes Supplemental Experimental Procedures, three figures, and one table and can be found with this article online at doi:10.1016/j.cmet.2011.02.010.

ACKNOWLEDGMENTS

We thank F. Takahashi, Y. Kanto, R. Hoshino, and Y. Kishida for their excellent technical assistance. This work was supported by a grant from TSBMI from the Ministry of Education, Culture, Sports, Science and Technology of Japan (to T.K.), a Grant-in-aid for Scientific Research in Priority Areas (S) from the

Ministry of Education, Culture, Sports, Science, and Technology of Japan (to T.K.), a Grant-in-aid for Scientific Research from the Ministry of Health, Labor, and Welfare (to K.U.), Health Science Research grants (Research on Human Genome and Gene Therapy) from the Ministry of Health and Welfare (to T.K.), and a grant from Takeda Science Foundation (to K.U.).

Received: July 1, 2010

Revised: December 17, 2010

Accepted: February 3, 2011

Published: April 5, 2011

REFERENCES

- Awazawa, M., Ueki, K., Inabe, K., Yamauchi, T., Kaneko, K., Okazaki, Y., Bardeesy, N., Ohnishi, S., Nagai, R., and Kadowaki, T. (2009). Adiponectin suppresses hepatic SREBP1c expression in an AdipoR1/LKB1/AMPK dependent pathway. *Biochem. Biophys. Res. Commun.* **382**, 51–56.
- Berg, A.H., Combs, T.P., Du, X., Brownlee, M., and Scherer, P.E. (2001). The adipocyte-secreted protein Acrp30 enhances hepatic insulin action. *Nat. Med.* **7**, 947–953.
- Cressman, D.E., Greenbaum, L.E., DeAngelis, R.A., Ciliberto, G., Furth, E.E., Poli, V., and Taub, R. (1996). Liver failure and defective hepatocyte regeneration in interleukin-6-deficient mice. *Science* **274**, 1379–1383.
- Denzel, M.S., Scimia, M.-C., Zumstein, P.M., Walsh, K., Ruiz-Lozano, P., and Ranscht, B. (2010). T-cadherin is critical for adiponectin-mediated cardioprotection in mice. *J. Clin. Invest.* **120**, 4342–4352.
- Devaraj, S., Torok, N., Dasu, M.R., Samols, D., and Jialal, I. (2008). Adiponectin decreases C-reactive protein synthesis and secretion from endothelial cells: evidence for an adipose tissue-vascular loop. *Arterioscler. Thromb. Vasc. Biol.* **28**, 1368–1374.
- Dong, X., Park, S., Lin, X., Copps, K., Yi, X., and White, M.F. (2006). Irs1 and Irs2 signaling is essential for hepatic glucose homeostasis and systemic growth. *J. Clin. Invest.* **116**, 101–114.
- Ernst, M., Inglese, M., Waring, P., Campbell, I.K., Bao, S., Clay, F.J., Alexander, W.S., Wicks, I.P., Tarlinton, D.M., Novak, U., et al. (2001). Defective gp130-mediated signal transducer and activator of transcription (STAT) signaling results in degenerative joint disease, gastrointestinal ulceration, and failure of uterine implantation. *J. Exp. Med.* **194**, 189–203.
- Fain, J.N., Madan, A.K., Hiler, M.L., Cheema, P., and Bahouth, S.W. (2004). Comparison of the release of adipokines by adipose tissue, adipose tissue matrix, and adipocytes from visceral and subcutaneous abdominal adipose tissues of obese humans. *Endocrinology* **145**, 2273–2282.
- Febbraio, M.A., Hiscock, N., Sacchetti, M., Fischer, C.P., and Pedersen, B.K. (2004). Interleukin-6 is a novel factor mediating glucose homeostasis during skeletal muscle contraction. *Diabetes* **53**, 1643–1648.
- Friedman, J.R., Larris, B., Le, P.P., Peiris, T.H., Arsenlis, A., Schug, J., Tobias, J.W., Kaestner, K.H., and Greenbaum, L.E. (2004). Orthogonal analysis of C/EBPbeta targets in vivo during liver proliferation. *Proc. Natl. Acad. Sci. USA* **101**, 12986–12991.
- Fruebis, J., Tsao, T.-S., Javorschi, S., Ebbets-Reed, D., Erickson, M.R.S., Yen, F.T., Bihain, B.E., and Lodish, H.F. (2001). Proteolytic cleavage product of 30-kDa adipocyte complement-related protein increases fatty acid oxidation in muscle and causes weight loss in mice. *Proc. Natl. Acad. Sci. USA* **98**, 2005–2010.
- Guo, S., Copps, K.D., Dong, X., Park, S., Cheng, Z., Pocai, A., Rossetti, L., Sajjan, M., Farese, R.V., and White, M.F. (2009). The Irs1 branch of the insulin signaling cascade plays a dominant role in hepatic nutrient homeostasis. *Mol. Cell. Biol.* **29**, 5070–5083.
- Haugen, F., and Drevon, C.A. (2007). Activation of nuclear factor-kappaB by high molecular weight and globular adiponectin. *Endocrinology* **148**, 5478–5486.
- Holmes, A.G., Mesa, J.L., Neill, B.A., Chung, J., Carey, A.L., Steinberg, G.R., Kemp, B.E., Southgate, R.J., Lancaster, G.I., Bruce, C.R., et al. (2008). Prolonged interleukin-6 administration enhances glucose tolerance and increases skeletal muscle PPARalpha and UCP2 expression in rats. *J. Endocrinol.* **198**, 367–374.
- Hotamisligil, G.S., Peraldi, P., Budavari, A., Ellis, R., White, M.F., and Spiegelman, B.M. (1996). IRS-1-mediated inhibition of insulin receptor tyrosine kinase activity in TNF-alpha- and obesity-induced insulin resistance. *Science* **271**, 665–668.
- Huang, H., Park, P.H., McMullen, M.R., and Nagy, L.E. (2008). Mechanisms for the anti-inflammatory effects of adiponectin in macrophages. *J. Gastroenterol. Hepatol.* **23** (Suppl 1), S50–S53.
- Hug, C., Wang, J., Ahmad, N.S., Bogan, J.S., Tsao, T.-S., and Lodish, H.F. (2004). T-cadherin is a receptor for hexameric and high-molecular-weight forms of Acrp30/adiponectin. *Proc. Natl. Acad. Sci. USA* **101**, 10308–10313.
- Ichikawa, M., Goyama, S., Asai, T., Kawazu, M., Nakagawa, M., Takeshita, M., Chiba, S., Ogawa, S., and Kurokawa, M. (2008). AML1/Runx1 negatively regulates quiescent hematopoietic stem cells in adult hematopoiesis. *J. Immunol.* **180**, 4402–4408.
- Ide, T., Shimano, H., Yahagi, N., Matsuzaka, T., Nakakuki, M., Yamamoto, T., Nakagawa, Y., Takahashi, A., Suzuki, H., Sone, H., et al. (2004). SREBPs suppress IRS-2-mediated insulin signalling in the liver. *Nat. Cell Biol.* **6**, 351–357.
- Inoue, H., Ogawa, W., Ozaki, M., Haga, S., Matsumoto, M., Furukawa, K., Hashimoto, N., Kido, Y., Mori, T., Sakaue, H., et al. (2004). Role of STAT-3 in regulation of hepatic gluconeogenic genes and carbohydrate metabolism in vivo. *Nat. Med.* **10**, 168–174.
- Ivanov, D., Philippova, M., Antropova, J., Gubaeva, F., Iljinskaya, O., Tararak, E., Bochkov, V., Erne, P., Resink, T., and Tkachuk, V. (2001). Expression of cell adhesion molecule T-cadherin in the human vasculature. *Histochem. Cell Biol.* **115**, 231–242.
- Iwabu, M., Yamauchi, T., Okada-Iwabu, M., Sato, K., Nakagawa, T., Funata, M., Yamaguchi, M., Namiki, S., Nakayama, R., Tabata, M., et al. (2010). Adiponectin and AdipoR1 regulate PGC-1alpha and mitochondria by Ca(2+) and AMPK/SIRT1. *Nature* **464**, 1313–1319.
- Jhala, U.S., Canettieri, G., Srean, R.A., Kulkarni, R.N., Krajewski, S., Reed, J., Walker, J., Lin, X., White, M., and Montminy, M. (2003). cAMP promotes pancreatic beta-cell survival via CREB-mediated induction of IRS2. *Genes Dev.* **17**, 1575–1580.
- Kadowaki, T., Yamauchi, T., Kubota, N., Hara, K., Ueki, K., and Tobe, K. (2006). Adiponectin and adiponectin receptors in insulin resistance, diabetes, and the metabolic syndrome. *J. Clin. Invest.* **116**, 1784–1792.
- Kamei, N., Tobe, K., Suzuki, R., Ohsugi, M., Watanabe, T., Kubota, N., Ohtsuka-Kowatari, N., Kumagai, K., Sakamoto, K., Kobayashi, M., et al. (2006). Overexpression of monocyte chemoattractant protein-1 in adipose tissues causes macrophage recruitment and insulin resistance. *J. Biol. Chem.* **281**, 26602–26614.
- Kelly, M., Gauthier, M.-S., Saha, A.K., and Ruderman, N.B. (2009). Activation of AMP-activated protein kinase by interleukin-6 in rat skeletal muscle: association with changes in cAMP, energy state, and endogenous fuel mobilization. *Diabetes* **58**, 1953–1960.
- Kershaw, E.E., and Flier, J.S. (2004). Adipose tissue as an endocrine organ. *J. Clin. Endocrinol. Metab.* **89**, 2548–2556.
- Kubota, N., Tobe, K., Terauchi, Y., Eto, K., Yamauchi, T., Suzuki, R., Tsubamoto, Y., Komeda, K., Nakano, R., Miki, H., et al. (2000). Disruption of insulin receptor substrate 2 causes type 2 diabetes because of liver insulin resistance and lack of compensatory beta-cell hyperplasia. *Diabetes* **49**, 1880–1889.
- Kubota, N., Terauchi, Y., Yamauchi, T., Kubota, T., Moroi, M., Matsui, J., Eto, K., Yamashita, T., Kamon, J., Satoh, H., et al. (2002). Disruption of adiponectin causes insulin resistance and neointimal formation. *J. Biol. Chem.* **277**, 25863–25866.
- Kubota, N., Kubota, T., Itoh, S., Kumagai, H., Kozono, H., Takamoto, I., Mineyama, T., Ogata, H., Tokuyama, K., Ohsugi, M., et al. (2008). Dynamic functional relay between insulin receptor substrate 1 and 2 in hepatic insulin signaling during fasting and feeding. *Cell Metab.* **8**, 49–64.

- Levy, D.E., and Darnell, J.E., Jr. (2002). Stats: transcriptional control and biological impact. *Nat. Rev. Mol. Cell Biol.* 3, 651–662.
- Libermann, T.A., and Baltimore, D. (1990). Activation of interleukin-6 gene expression through the NF-kappa B transcription factor. *Mol. Cell. Biol.* 10, 2327–2334.
- Pedersen, B.K., and Febbraio, M.A. (2008). Muscle as an endocrine organ: focus on muscle-derived interleukin-6. *Physiol. Rev.* 88, 1379–1406.
- Pradhan, A.D., Manson, J.E., Rifai, N., Buring, J.E., and Ridker, P.M. (2001). C-reactive protein, interleukin 6, and risk of developing type 2 diabetes mellitus. *JAMA* 286, 327–334.
- Rovin, B.H., and Song, H. (2006). Chemokine induction by the adipocyte-derived cytokine adiponectin. *Clin. Immunol.* 120, 99–105.
- Ruan, H., Zarnowski, M.J., Cushman, S.W., and Lodish, H.F. (2003). Standard isolation of primary adipose cells from mouse epididymal fat pads induces inflammatory mediators and down-regulates adipocyte genes. *J. Biol. Chem.* 278, 47585–47593.
- Shimomura, I., Matsuda, M., Hammer, R.E., Bashmakov, Y., Brown, M.S., and Goldstein, J.L. (2000). Decreased IRS-2 and increased SREBP-1c lead to mixed insulin resistance and sensitivity in livers of lipodystrophic and ob/ob mice. *Mol. Cell* 6, 77–86.
- Sun, X.J., Wang, L.-M., Zhang, Y., Yenush, L., Myers, M.G., Jr., Glasheen, E., Lane, W.S., Pierce, J.H., and White, M.F. (1995). Role of IRS-2 in insulin and cytokine signalling. *Nature* 377, 173–177.
- Tamemoto, H., Kadowaki, T., Tobe, K., Yagi, T., Sakura, H., Hayakawa, T., Terauchi, Y., Ueki, K., Kaburagi, Y., Satoh, S., et al. (1994). Insulin resistance and growth retardation in mice lacking insulin receptor substrate-1. *Nature* 372, 182–186.
- Taniguchi, C.M., Emanuelli, B., and Kahn, C.R. (2006). Critical nodes in signaling pathways: insights into insulin action. *Nat. Rev. Mol. Cell Biol.* 7, 85–96.
- Torisu, T., Sato, N., Yoshiga, D., Kobayashi, T., Yoshioka, T., Mori, H., Iida, M., and Yoshimura, A. (2007). The dual function of hepatic SOCS3 in insulin resistance in vivo. *Genes Cells* 12, 143–154.
- Tsao, T.-S., Murrey, H.E., Hug, C., Lee, D.H., and Lodish, H.F. (2002). Oligomerization state-dependent activation of NF-kappa B signaling pathway by adipocyte complement-related protein of 30 kDa (Acrp30). *J. Biol. Chem.* 277, 29359–29362.
- Tsao, T.-S., Tomas, E., Murrey, H.E., Hug, C., Lee, D.H., Ruderman, N.B., Heuser, J.E., and Lodish, H.F. (2003). Role of disulfide bonds in Acrp30/adiponectin structure and signaling specificity. Different oligomers activate different signal transduction pathways. *J. Biol. Chem.* 278, 50810–50817.
- Ueki, K., Algenstaedt, P., Mauvais-Jarvis, F., and Kahn, C.R. (2000). Positive and negative regulation of phosphoinositide 3-kinase-dependent signaling pathways by three different gene products of the p85alpha regulatory subunit. *Mol. Cell. Biol.* 20, 8035–8046.
- Waki, H., Yamauchi, T., Kamon, J., Kita, S., Ito, Y., Hada, Y., Uchida, S., Tsuchida, A., Takekawa, S., and Kadowaki, T. (2005). Generation of globular fragment of adiponectin by leukocyte elastase secreted by monocytic cell line THP-1. *Endocrinology* 146, 790–796.
- Yamada, Y., Kirillova, I., Peschon, J.J., and Fausto, N. (1997). Initiation of liver growth by tumor necrosis factor: deficient liver regeneration in mice lacking type I tumor necrosis factor receptor. *Proc. Natl. Acad. Sci. USA* 94, 1441–1446.
- Yamauchi, T., Kamon, J., Waki, H., Terauchi, Y., Kubota, N., Hara, K., Mori, Y., Ide, T., Murakami, K., Tsuboyama-Kasaoka, N., et al. (2001). The fat-derived hormone adiponectin reverses insulin resistance associated with both lipodystrophy and obesity. *Nat. Med.* 7, 941–946.
- Yamauchi, T., Kamon, J., Minokoshi, Y., Ito, Y., Waki, H., Uchida, S., Yamashita, S., Noda, M., Kita, S., Ueki, K., et al. (2002). Adiponectin stimulates glucose utilization and fatty-acid oxidation by activating AMP-activated protein kinase. *Nat. Med.* 8, 1288–1295.
- Yamauchi, T., Kamon, J., Ito, Y., Tsuchida, A., Yokomizo, T., Kita, S., Sugiyama, T., Miyagishi, M., Hara, K., Tsunoda, M., et al. (2003). Cloning of adiponectin receptors that mediate antidiabetic metabolic effects. *Nature* 423, 762–769.
- Yamauchi, T., Nio, Y., Maki, T., Kobayashi, M., Takazawa, T., Iwabu, M., Okada-Iwabu, M., Kawamoto, S., Kubota, N., Kubota, T., et al. (2007). Targeted disruption of AdipoR1 and AdipoR2 causes abrogation of adiponectin binding and metabolic actions. *Nat. Med.* 13, 332–339.
- Zhang, P., Wang, Y., Fan, Y., Tang, Z., and Wang, N. (2009). Overexpression of adiponectin receptors potentiates the antiinflammatory action of subeffective dose of globular adiponectin in vascular endothelial cells. *Arterioscler. Thromb. Vasc. Biol.* 29, 67–74.

Thiazolidinediones Enhance Sodium-Coupled Bicarbonate Absorption from Renal Proximal Tubules via PPAR γ -Dependent Nongenomic Signaling

Yoko Endo,¹ Masashi Suzuki,¹ Hideomi Yamada,¹ Shoko Horita,¹ Motoei Kunimi,¹ Osamu Yamazaki,¹ Ayumi Shirai,¹ Motonobu Nakamura,¹ Naoyuki Iso-O,¹ Yuehong Li,^{1,3} Masumi Hara,¹ Kazuhisa Tsukamoto,¹ Nobuo Moriyama,⁴ Akihiko Kudo,⁵ Hayato Kawakami,⁵ Toshimasa Yamauchi,¹ Naoto Kubota,¹ Takashi Kadowaki,¹ Haruki Kume,² Yutaka Enomoto,² Yukio Homma,² George Seki,^{1,*} and Toshiro Fujita¹

¹Department of Internal Medicine

²Department of Urology, Faculty of Medicine

University of Tokyo, 7-3-1 Bunkyo-ku, Hongo, Tokyo 113-0033, Japan

³Department of Nephrology, People's Hospital, Peking University, 11 Xizhimen South Street, Beijing 100044, China

⁴Department of Experimental Nursing, Faculty of Nursing, Fukuoka Prefectural University, Tagawa-shi, Ida 4395, Fukuoka 825-8585, Japan

⁵Department of Anatomy, Kyorin University School of Medicine, 6-20-2 Shinkawa, Mitaka, Tokyo 181-8611, Japan

*Correspondence: georgeseki-tyk@umin.ac.jp

DOI 10.1016/j.cmet.2011.02.015

SUMMARY

Thiazolidinediones (TZDs) improve insulin resistance by activating a nuclear hormone receptor, peroxisome proliferator-activated receptor γ (PPAR γ). However, the use of TZDs is associated with plasma volume expansion through a mechanism that remains to be clarified. Here we showed that TZDs rapidly stimulate sodium-coupled bicarbonate absorption from the renal proximal tubule *in vitro* and *in vivo*. TZD-induced transport stimulation is dependent on PPAR γ -Src-EGFR-ERK and observed in rat, rabbit and human, but not in mouse proximal tubules where Src-EGFR is constitutively activated. The existence of PPAR γ -Src-dependent nongenomic signaling, which requires the ligand-binding ability, but not the transcriptional activity of PPAR γ , is confirmed in mouse embryonic fibroblast cells. The enhancement of the association between PPAR γ and Src by TZDs supports an indispensable role of Src in this signaling. These results suggest that the PPAR γ -dependent nongenomic stimulation of renal proximal transport is also involved in TZD-induced volume expansion.

INTRODUCTION

Peroxisome proliferator-activated receptor γ (PPAR γ) is a ligand-activated transcription factor that belongs to the nuclear hormone receptor gene superfamily (Yki-Järvinen, 2004). Pharmacological activation of PPAR γ by thiazolidinediones (TZDs) such as rosiglitazone (RGZ) and pioglitazone (PGZ) significantly improves insulin resistance and lowers plasma glucose concentrations (Yki-Järvinen, 2004). TZDs may also have beneficial effects on the cardiovascular system, including the reduction of blood pressure and the improvement of vascular function

(Ryan et al., 2004). However, fluid retention, one of the main side effects of TZDs, precludes the use of TZDs in the setting of severe heart failure (Mudaliar et al., 2003).

While the enhancement of sodium and fluid reabsorption from the kidney, in addition to the peripheral vasodilatation, may contribute to TZD-induced edema formation, the molecular mechanism underlying the renal tubular actions of TZDs has been a matter of controversy. Thus, the studies on mice with the selective deletion of PPAR γ from renal collecting ducts originally suggested that TZD-induced volume expansion is dependent on transport stimulation in the distal nephrons (Guan et al., 2005; Zhang et al., 2005). In particular, the PPAR γ -mediated enhanced transcription of the epithelial Na channel (ENaC) γ subunit was thought to play a key role (Guan et al., 2005; Zhang et al., 2005). TZDs might also enhance the surface expression of ENaC α subunit through the glucocorticoid-inducible kinase SGK1 (Hong et al., 2003). However, other studies did not support a central role of the ENaC in TZD-induced fluid retention. For example, TZDs did not alter basal and insulin-stimulated ENaC activities in well-established renal principal cell culture models (Nofziger et al., 2005). In addition, TZDs did not consistently enhance the expression of ENaC subunits (Song et al., 2004). While an ENaC inhibitor, amiloride, prevented TZD-induced volume expansion in mice (Guan et al., 2005), it failed to prevent volume expansion in rats induced by a non-TZD PPAR γ agonist, GI262570 (Chen et al., 2005). Furthermore, TZD-induced fluid retention was not suppressed in mice lacking ENaC α subunit selectively in collecting ducts (Vallon et al., 2009), strongly suggesting that the enhancement of ENaC activity alone cannot explain TZD-induced volume expansion. On the other hand, both human (Zanchi et al., 2004) and animal (Muto et al., 2001) studies suggested that renal proximal tubule (PT) transport could be stimulated by TZDs. We reasoned that TZD-induced volume expansion is multifactorial and that PTs may be another target nephron segment of TZDs.

In the present study we demonstrate that TZDs markedly stimulate *in vitro* and *in vivo* PT transport. This rapid transport stimulation is dependent on PPAR γ -Src-EGFR-ERK and observed in isolated PTs from rabbit, rat, and human. In mouse

PTs, however, TZDs fail to induce transport stimulation probably because of the unique constitutive activity of Src. The existence of PPAR γ -Src-dependent nongenomic signaling, which requires the ligand-binding ability, but not the transcriptional activity, of PPAR γ is confirmed in mouse embryonic fibroblast (EF) cells. Furthermore, TZDs rapidly enhance the association between PPAR γ and Src, supporting an indispensable role of Src in this signaling. We propose that, in addition to enhanced expression of sodium transporter(s) through the PPAR γ -dependent genomic signaling, the stimulation of renal PT transport through the PPAR γ -dependent nongenomic signaling is also involved in TZD-induced volume expansion.

RESULTS

Effects of TZDs on Transport Functions in Isolated Rabbit PTs

To examine whether TZDs can stimulate PT transport, we first focused on the acute effects of TZDs on the electrogenic Na⁺-HCO₃⁻ cotransporter NBCe1 that mediates the majority of Na⁺-coupled HCO₃⁻ absorption from PTs (Li et al., 2008). In isolated lumenally collapsed rabbit PTs, 0.3 μ M PGZ markedly stimulated the NBCe1 activity within minutes (Figure 1A). Both PGZ and RGZ stimulated the NBCe1 activity at submicromolar, but not micromolar concentrations (Figures 1B and 1C). We next examined the effects of TZDs on the activity of luminal Na⁺/H⁺ exchanger NHE3 in lumenally perfused PTs and found that 0.3 μ M PGZ markedly stimulated the NHE3 activity (Figures S1A and S1B, available online). Submicromolar concentrations of PGZ also enhanced the rate of HCO₃⁻ absorption (JHCO₃⁻) within 5 min (Figure 1D), indicating that TZDs can acutely stimulate the net Na⁺ and HCO₃⁻ absorption from PTs by enhancing the activities of both NBCe1 and NHE3.

To examine the signaling mechanism of TZD-induced stimulation of PT transport, we used a tyrosine kinase inhibitor, genistein (20 μ M), a MEK inhibitor, PD98059 (10 μ M), a PPAR γ antagonist, GW9662 (5 μ M), an EGFR tyrosine kinase inhibitor, AG1478 (20 μ M), a PKC inhibitor, calphostin C (0.5 μ M), and a PKA inhibitor, H89 (10 μ M). All of these inhibitors did not change the basal JHCO₃⁻ values at the concentrations used in this study. While genistein, PD98059, GW9662, and AG1478 largely suppressed the PGZ-induced stimulation of JHCO₃⁻, calphostin C and H89 were without effects (Figure 1E). PGZ also rapidly stimulated ERK phosphorylation in renal cortex tissues that was abolished by AG1478, GW9662, and PD98059 (Figure 1F). These results indicate that, among multiple rapid signaling pathways that are potentially activated by TZDs (Burgermeister and Seger, 2008), the EGFR/ERK pathway is critically involved in the effects of TZDs on PT transport. To confirm the involvement of PPAR γ in TZD-induced PT transport stimulation, we performed immunohistochemical analysis on rabbit kidneys. In addition to the intense PPAR γ expression in inner medullary collecting ducts as reported (Guan et al., 1997), the diffuse cytosolic expression of PPAR γ in PTs was also evident (Figure 1G). Western blot analysis confirmed the expression of PPAR γ protein in both medulla and cortex (Figure 1H). Together with the suppression of TZD-induced PT transport stimulation by GW9662, these results support a view that PPAR γ -dependent signaling is involved in

the TZD-induced stimulation of PT transport. The specificity of mouse and rabbit anti-PPAR γ antibodies is shown in Figure S1C.

Species Differences in TZD's Effects on PT Transport

In view of potential species differences in the mechanism of TZD-induced fluid retention (Chen et al., 2005; Guan et al., 2005), we next examined the effects of TZDs on PT transport in the different species. PGZ at 0.3 μ M stimulated NBCe1 activity in rats to a similar extent as in rabbits. However, the stimulatory effect of PGZ was absent in mice (Figure 2A). In mouse PTs, PGZ at concentrations from 0.003 to 3 μ M failed to stimulate JHCO₃⁻ (Figure 2B). Because both rat and mouse PTs express PPAR γ (Figures 2C and 2D), the lack of transport stimulation by TZDs in mouse PTs cannot be attributable to the absence of PPAR γ .

On the other hand, an Src inhibitor, PP2 (3 μ M), completely suppressed the stimulatory effect of PGZ on NBCe1 activity in rabbit PTs (Figure 2E), consistent with the involvement of Src in TZD-induced stimulation of PT transport. Interestingly, mouse PTs were reported to have the unique constitutive activity of Src, which was not found either in other mouse tissues or in PTs of other species (Kiley and Chevalier, 2007). We hypothesized that the constitutive activation of Src, together with the dysregulation of downstream EGFR signaling (Kiley and Chevalier, 2007), might be responsible for the lack of stimulatory effect of TZDs in mouse PTs. Although PGZ stimulated renal cortex Src phosphorylation in rabbits and rats, it failed to induce Src phosphorylation in mice, presumably because of the highly phosphorylated basal status (Figure 2F). PGZ also stimulated ERK phosphorylation in rats, but not in mice because of the basal activation (Figure 2G). These results suggest that the constitutive activation of Src, which abolishes the estrogen receptor (ER)-mediated nongenomic activation of endothelial NO synthase (eNOS) (Li et al., 2007), also interferes with the PPAR γ -mediated nongenomic signaling. In rat renal cortex, the PGZ-induced Src phosphorylation was suppressed by PP2, but not by AG1478. On the other hand, the PGZ-induced EGFR phosphorylation was suppressed by both PP2 and AG1478 (Figure S2). These results indicate that Src acts upstream of EGFR in the TZD-induced signaling.

Notably, human PTs do not have the constitutive activation of Src (Kiley and Chevalier, 2007) and hence may be sensitive to the stimulatory effect of TZDs. Indeed, 0.3 μ M PGZ markedly stimulated the NBCe1 activity in isolated human PTs, and this stimulation was totally suppressed by PD98059 and GW9662 (Figure 3A). Immunohistochemical analysis revealed that PPAR γ was diffusely expressed in human PTs (Figure 3B). Furthermore, western blot analysis confirmed the expression of PPAR γ protein in isolated human PTs (Figure 3C).

Acute In Vivo Effects of TZDs

To examine whether the TZD-induced stimulation of PT transport modifies whole-body volume homeostasis, we performed acute clearance studies in water-loaded conscious rats. Rats were orally given PGZ at a single dose of 10 mg/kg body weight (BW) and urine was collected for over 90 min. Taking account of the high affinity of PGZ to plasma proteins, this protocol is estimated to keep the protein-unbound, plasma PGZ concentration at around 0.3 μ M for at least 2 hr (Krieter et al., 1994). PGZ

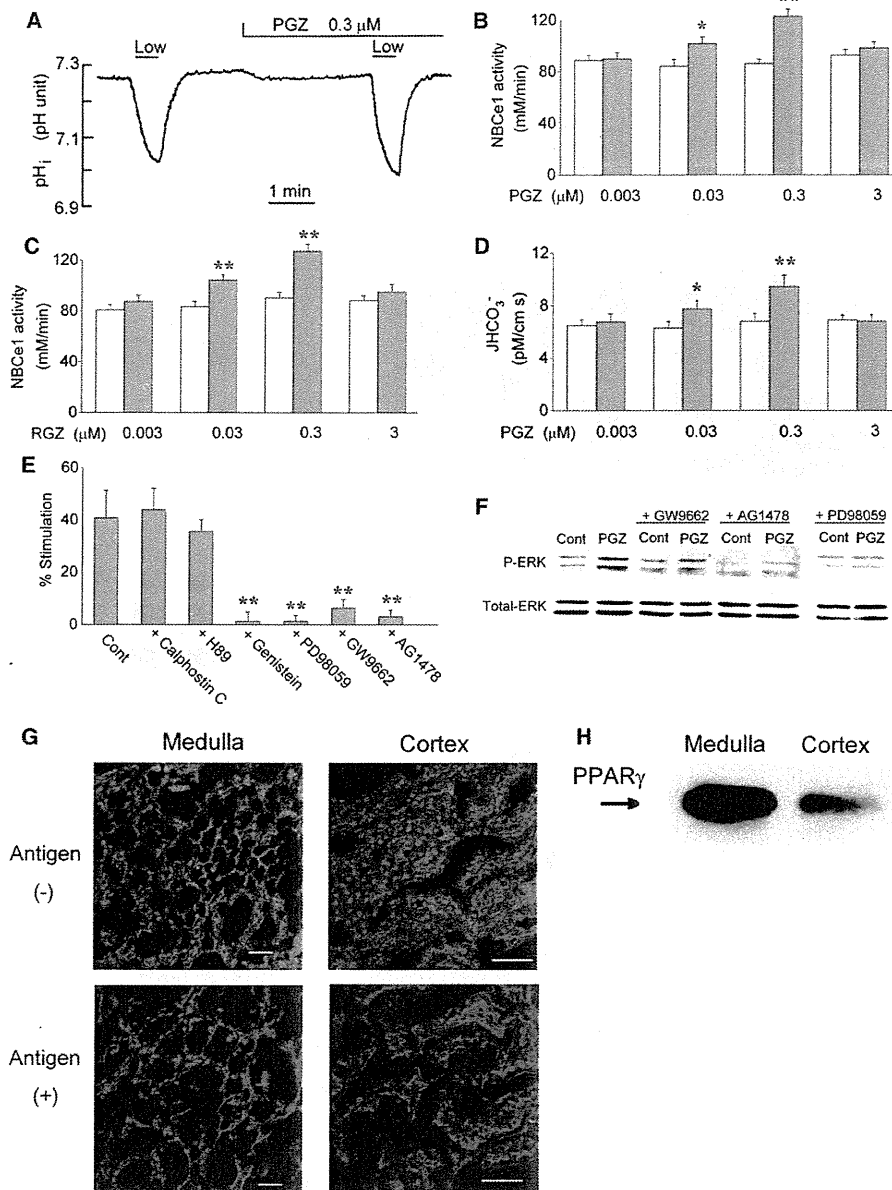


Figure 1. Stimulation of PT Transport by TZDs through PPAR γ -Dependent Pathway in Rabbits

(A) pH_i responses to bath HCO₃⁻ reduction from 25 to 12.5 mM (indicated as Low) in isolated rabbit PT.

(B) Concentration dependency of PGZ effects on NBCe1 activity. Open bars represent the control activities and closed bars represent the activities 5 min after the addition of PGZ. *p < 0.05 versus control; **p < 0.01 versus control. Data are means \pm SEM. Each n = 7.

(C) Concentration dependency of RGZ effects on NBCe1 activity. **p < 0.01 versus control. Data are means \pm SEM. Each n = 7.

(D) Concentration dependency of PGZ effects on the rate of JHCO₃⁻. Open bars represent the control fluxes and closed bars represent the fluxes 5 min after the addition of PGZ. *p < 0.05 versus control; **p < 0.01 versus control. Data are means \pm SEM. Each n = 7.

(E) Roles of protein kinases and PPAR γ in the stimulation of JHCO₃⁻ by PGZ. Tubules were incubated with these inhibitors for 20 min. **p < 0.01 versus control. Data are means \pm SEM of six to eight experiments.

(F) ERK phosphorylation in rabbit renal cortex tissues. The samples were incubated for 40 min in the absence or presence of inhibitors and 0.3 μ M PGZ was added for 5 min. Total ERK and P-ERK were detected.

(G) Immunohistochemical analysis of PPAR γ expression in rabbit kidney. The goat anti-PPAR γ antibody was applied in the absence or presence of antigen (10 mg/L). Images are shown in pseudocolor, where green shows PPAR γ , red shows actin, and blue shows nuclei. Bars = 50 μ m.

(H) Western blot analysis on rabbit kidney with the mouse anti-PPAR γ antibody. Each lane contained 20 μ g of protein. See also Figure S1.

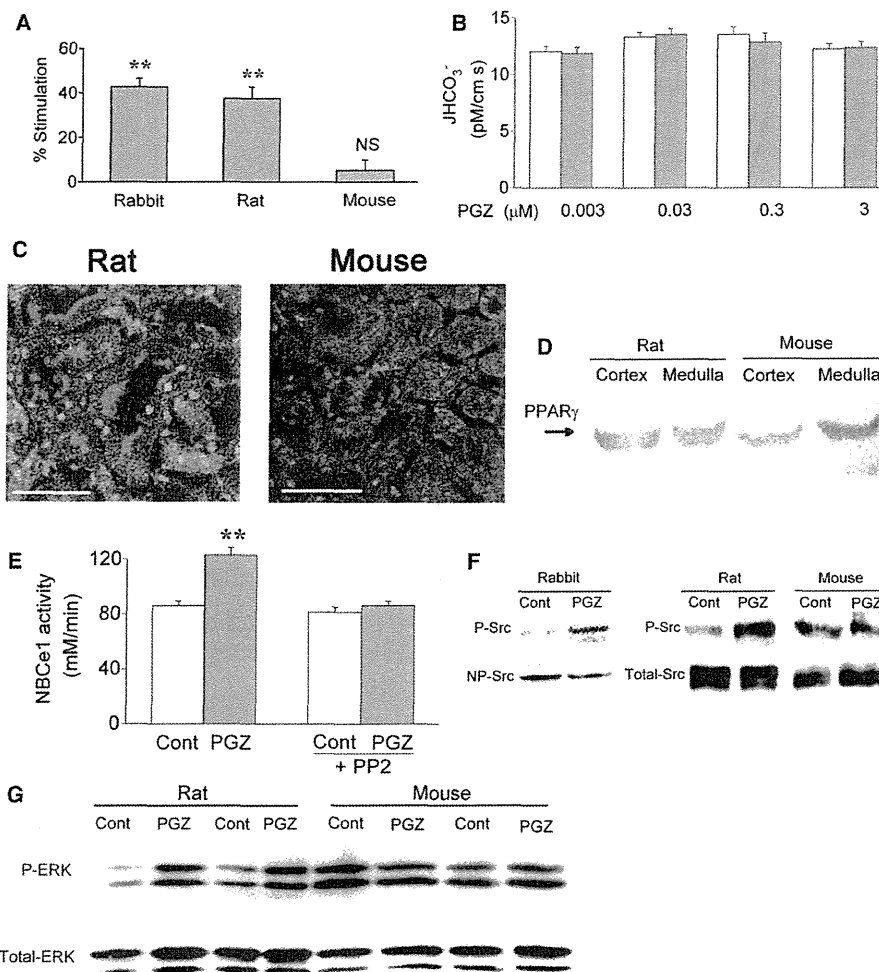


Figure 2. Species Difference in Effects of TZDs on PT Transport

(A) Effects of 0.3 μM PGZ on NBCe1 activity in rabbit, rat, or mouse. ** $p < 0.01$ versus control. Data are means \pm SEM of seven to eight experiments. NS, not significant.

(B) Concentration dependency of PGZ effects on JHCO_3^- in mouse. Open bars represent the control fluxes and closed bars represent the fluxes 5 min after the addition of PGZ. Data are means \pm SEM. Each $n = 6$.

(C) Immunohistochemical analysis of PPAR γ expression in rat and mouse kidneys. Details are as in Figure 1G, but the rabbit anti-PPAR γ antibody was used. Bars = 50 μm .

(D) Western blot analysis on rat and mouse kidneys with the rabbit anti-PPAR γ antibody. Each lane contained 20 μg of protein.

(E) Effects of 0.3 μM PGZ on NBCe1 activity in isolated rabbit PTs in the absence and presence of Src inhibitor PP2 (3 μM). Open bars represent the control activities and closed bars represent the activities 5 min after the addition of PGZ. ** $p < 0.01$ versus control. Data are means \pm SEM. Each $n = 7$.

(F) Src phosphorylation in renal cortex tissues. The samples were treated with 0.3 μM PGZ for 5 min. Total Src, nonphosphorylated Src (NP-Src), and phosphorylated Src (P-Src) were detected.

(G) ERK phosphorylation in rat and mouse renal cortex tissues. Details are as in Figure 1F. See also Figure S2.

significantly reduced urinary volume (UV), fractional excretion of lithium (FELi⁺), and free water clearance (CH₂O) without changing creatinine clearance (CCR) or urinary sodium excretion (UNaV) (Figure 4A). PGZ also slightly increased urinary osmolality (Uosm), which could be explained by the stimulation of PT absorption and the resultant decrease in delivery of water and electrolytes to the loop of Henle (de Rouffignac et al., 1991). Consistent with this interpretation, the simultaneous administra-

tion of a PT transport inhibitor, acetazolamide (ACZ), with PGZ abolished the changes in UV, FELi⁺, CH₂O, and Uosm. Systolic blood pressure, analyzed by tail-cuff measurement, was unaffected by PGZ (Figure S3A). Mild sodium depletion during the acute clearance studies seemed to be responsible for the lack of PGZ effect on UNaV. Indeed, PGZ significantly reduced UV, FELi⁺, CH₂O, as well as UNaV, and increased Uosm when rats were loaded with half saline (0.45% NaCl) instead of water

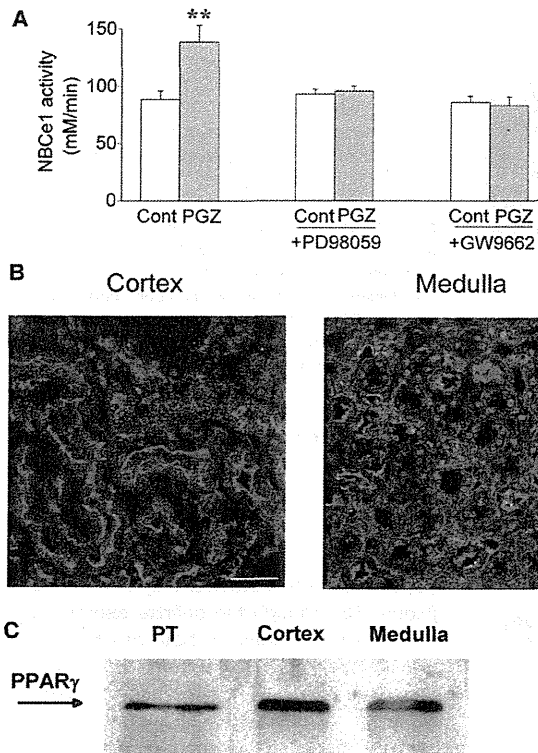


Figure 3. Effects of PGZ on Human PTs

(A) Effects of 0.3 μ M PGZ on NBCe1 activity in isolated human PTs. Open bars represent the control activities and closed bars represent the activities 5 min after the addition of PGZ. ** $p < 0.01$ versus control. Data are means \pm SEM of six to eight experiments.

(B) Immunohistochemical analysis of PPAR γ expression in human kidney. Details are as in Figure 1G, but the rabbit anti-PPAR γ antibody was used. Bars = 50 μ m.

(C) Western blot analysis on human kidney with the rabbit anti-PPAR γ antibody. The left lane contained 30 PTs manually dissected from cortex slices and the middle and right lanes each contained 20 μ g of proteins.

(Figure S3B). Immunohistochemical analysis revealed that the *in vivo* administration of PGZ enhanced ERK phosphorylation in *in situ* PTs (Figure 4B), which was confirmed by western blot analysis on renal cortex samples (Figure 4C). These results indicate that TZDs can acutely induce fluid retention by stimulating *in vivo* PT reabsorption in rats through the ERK-dependent pathway. On the other hand, the chronic RGZ administration for 3 days in rats was reported to enhance the expression of collecting duct water channel protein AQP2 (Song et al., 2004). However, we confirmed that the acute administration of PGZ did not affect the expression of AQP2 in renal medulla (Figure 4D).

We also performed acute clearance studies in mice with the identical water-loading protocol ($n = 11$ for both control and PGZ). Consistent with the lack of transport stimulation in isolated mouse PT, the acute administration of PGZ did not reduce UV (control, $3.8 \pm 0.5 \mu\text{l}/10 \text{g BW}/\text{min}$ versus PGZ, $4.2 \pm 0.4 \mu\text{l}/10 \text{g BW}/\text{min}$), FELi⁺ (control, $19.1 \pm 2.4\%$ versus

PGZ, $21.8 \pm 4.0\%$) or CH₂O (control, $0.62 \pm 0.18 \mu\text{l}/10 \text{g BW}/\text{min}$ versus PGZ, $0.80 \pm 0.25 \mu\text{l}/10 \text{g BW}/\text{min}$) in mice.

PPAR γ -Dependent Stimulation of NHE1 Activity in EF Cells

To further examine the nature of the PPAR γ -dependent rapid signaling pathway, we took advantage of EF cells, the only viable cells available from PPAR $\gamma^{-/-}$ mice (Kubota et al., 1999) and focused on the regulation of NHE1, the ubiquitously expressed Na⁺/H⁺ exchanger that is rapidly stimulated by the ERK pathway (Haworth et al., 2003). The sustained intracellular acidosis stimulated the NHE1 activity in both wild-type and PPAR $\gamma^{-/-}$ cells (Figure 5A). This stimulation was totally suppressed by PD98059 (Figure 5B), indicating that the ERK-mediated NHE1 stimulation is intact in both cell types. On the other hand, 0.3 μ M PGZ rapidly stimulated the NHE1 activity in wild-type, but not in PPAR $\gamma^{-/-}$ cells (Figure 5C). In wild-type cells, PD98059, GW9662, and AG1478, but not a transcriptional inhibitor, actinomycin D, suppressed the PGZ-induced stimulation of NHE1 activity (Figure 5D). Furthermore, GW9662 and AG1478 suppressed the PGZ-induced ERK phosphorylation that was detected only in wild-type cells (Figure 5E). RGZ at 0.3 μ M also stimulated the NHE1 activity in wild-type cells by $79.9 \pm 10.4\%$ ($p < 0.01$, $n = 8$), but not in PPAR $\gamma^{-/-}$ cells. These results confirmed the existence of PPAR γ -dependent nongenomic signaling resulting in ERK activation in wild-type EF cells. They also support the previously proposed view that the constitutive activation of Src/ERK pathway is restricted to mouse PTs and is not found in other mouse tissues such as EF cells (Kiley and Chevalier, 2007).

In contrast to the stimulatory effect of submicromolar concentrations of TZDs, 30 μ M PGZ inhibited the NHE1 activity in both wild-type (control, $0.048 \pm 0.004 \text{ pH unit}/\text{min}$ versus PGZ, $0.029 \pm 0.002 \text{ pH unit}/\text{min}$, $p < 0.01$, $n = 7$) and PPAR $\gamma^{-/-}$ cells (control, $0.048 \pm 0.004 \text{ pH unit}/\text{min}$ versus PGZ, $0.028 \pm 0.003 \text{ pH unit}/\text{min}$, $p < 0.01$, $n = 7$). RGZ at 30 μ M also had a similar inhibitory effect on the NHE1 activity in both wild-type and PPAR $\gamma^{-/-}$ cells (Figure S4). Consistent with a previous study (Oliver et al., 2005), these results indicate that higher micromolar concentrations of TZDs inhibit NHE1 independently of PPAR γ as a class effect.

Nongenomic Nature of PPAR γ -Dependent Rapid Signaling in EF Cells

To examine whether the NHE1 stimulatory activity of PPAR γ can be discriminated from the gene transcriptional activity, we performed adenovirus-mediated transfer of mouse PPAR γ 1 constructs (Figure 6A) into PPAR $\gamma^{-/-}$ cells. As expected, the full-length PPAR γ was able to rescue the NHE1 stimulation and ERK phosphorylation by 0.3 μ M PGZ (Figures 6B and 6C). More importantly, the ligand-binding domain (LBD) construct, which lacks the entire N-terminal transcription activation function domain AF-1 and the DNA-binding domain, also rescued the NHE1 stimulation and ERK phosphorylation by 0.3 μ M PGZ (Figures 6D and 6E). However, the binding-deficient LBD mutant Q284P, corresponding to human Q286P (Saraf et al., 1999), failed to rescue the NHE1 stimulation or the ERK phosphorylation (Figures 6D and 6E). The failure of Q284P to rescue the PGZ-mediated

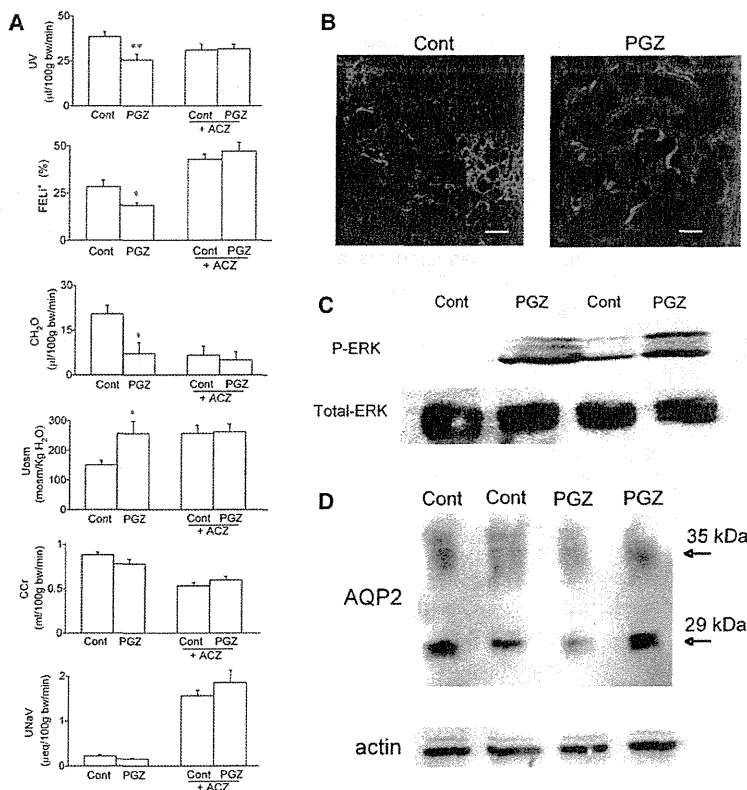


Figure 4. Effects of PGZ on In Vivo PT Transport in Rats

(A) Acute renal clearance study. Urine was collected for 90 min after a single oral dose of 10 mg/kg PGZ or vehicle. * $p < 0.05$ versus control; ** $p < 0.01$ versus control. Data are means \pm SEM of 11–12 experiments. Each $n = 7$.

(B) Effects of PGZ on ERK phosphorylation in rat kidneys in vivo. Sixty minutes after vehicle (Cont) or PGZ administration, kidneys were removed. Immunohistochemical analysis was performed with the antiphospho-ERK antibody. Green shows phosphorylated ERK, red shows actin, and blue shows nuclei. Bars = 50 μ m.

(C) Western blot analysis on rat kidney cortex with the anti-total ERK or the antiphosphorylated ERK antibody. Sixty minutes after vehicle (Cont) or PGZ administration, kidneys were removed. Each lane contained 20 μ g of proteins.

(D) Western blot analysis on rat kidney medulla with the anti-AQP2 or the anti-actin antibody. Details are as in (C). See also Figure S3.

NHE1 stimulation was not due to the altered intracellular expression, because the full-length PPAR γ , LBD, and Q284P showed an indistinguishable diffuse intracellular expression (Figure 6F). These results indicate that the NHE1 stimulatory activity requires the ligand-binding ability, but not the transcriptional activity, of PPAR γ . We confirmed that a 5 min incubation with PGZ did not change the pattern and level of intracellular PPAR γ expression.

To further confirm the dissociation of PPAR γ -mediated rapid signaling from gene transcription, we examined adipocyte differentiation, which absolutely requires the transcriptional activity of PPAR γ (Kubota et al., 1999; Tontonoz et al., 1994). The measurement of triglyceride (TG) contents revealed that wild-type, but not PPAR $\gamma^{-/-}$ cells had adipocyte differentiation ability (Figure S5). Whereas the full-length PPAR γ restored the ability of PPAR $\gamma^{-/-}$ cells to differentiate into adipocytes as reported (Kubota et al., 1999), LBD or Q284P failed to restore adipocyte differentiation (Figure S7). These results confirm that the PPAR γ -mediated rapid signaling can be dissociated from the gene transcriptional activity.

Roles of Src in PPAR γ -Dependent Rapid Signaling in EF Cells

To examine the roles of Src in TZD-induced stimulation of NHE1 activity, we next examined the effects of TZDs in EF cells derived from Src $^{-/-}$ mice (Klinghoffer et al., 1999). In Src $^{+/+}$ control cells, but not in Src $^{-/-}$ cells, 0.3 μ M PGZ stimulated the NHE1 activity (Figure 7A). The PGZ-induced ERK phosphor-

ylation was also detected only in Src $^{+/+}$ cells (Figure 7B), though the definite expression of PPAR γ was detected in both cell types (Figure 7C). These results confirm that Src is indispensable in PPAR γ -dependent nongenomic signaling.

In ER-mediated nongenomic signaling, the association between ER and Src was thought to play a key role (Li et al., 2007). Accordingly, we finally examined a possible interaction between PPAR γ and Src by coimmunoprecipitation assay. PPAR $\gamma^{-/-}$ cells were transfected with PPAR γ , and cell lysates were subjected to immunoprecipitation with anti-Src or anti-PPAR γ antibodies. We found that Src and PPAR γ coimmunoprecipitated each other and PGZ markedly enhanced this association (Figures 7D and 7E). PGZ also markedly stimulated the association between Src and LBD (Figure 7F). However, PGZ failed to enhance the association between Src and Q284P, indicating that the TZD-mediated recruitment of Src is dependent on the ligand-binding ability of PPAR γ .

DISCUSSION

In the present study we showed that TZDs markedly stimulated sodium-coupled bicarbonate absorption from isolated rabbit, rat, and human PTs by activating both NBCe1 and NHE3 through the PPAR γ /Src/EGFR/ERK pathway. Acute PGZ administration in rats induced the stimulation of in vivo PT transport. However, TZDs failed to stimulate in vitro and in vivo PT transport in mice, in which Src-EGFR-ERK is uniquely activated in a constitutive manner. Studies with EF cells confirmed the presence of a nongenomic signaling pathway depending on PPAR γ -Src-EGFR-ERK. Because the magnitude of enhancement in PT transport by TZDs was actually comparable to or even exceeded that by angiotensin II (Li et al., 2008), a hormone with the greatest stimulatory effect in this segment, we propose that the stimulation of renal PT transport through PPAR γ -dependent nongenomic signaling is involved, at least

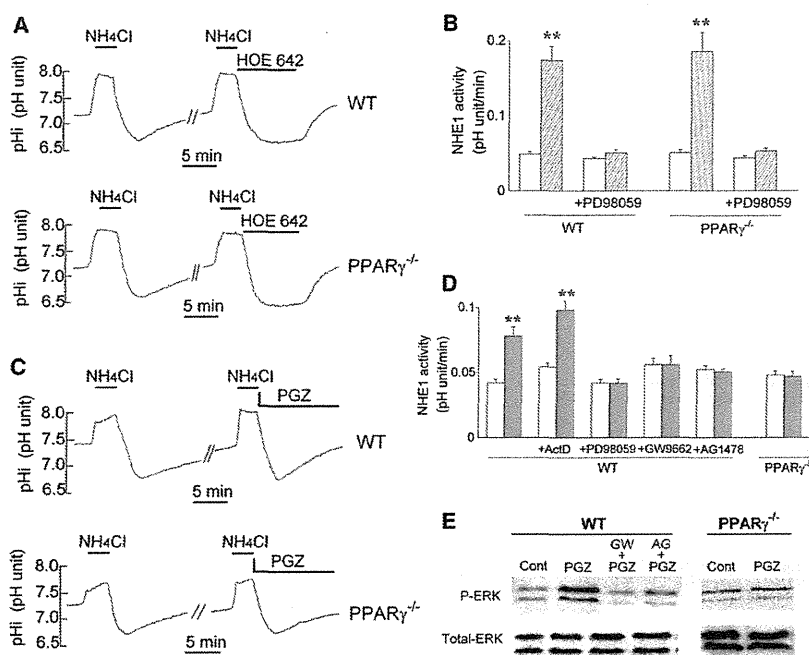


Figure 5. Effects of PGZ on NHE1 Activity in EF Cells

(A) The sustained intracellular acidosis induced by 3 μ M HOE642 stimulated the NHE1 activity in both wild-type (WT) and PPAR $\gamma^{-/-}$ cells.

(B) The ERK-dependent activation of NHE1 by sustained intracellular acidosis in EF cells. The NHE1 activity was estimated by the rate of pHi recovery at pHi of 6.9. Open bars represent the control activities and hatched bars represent the activities after intracellular acidosis. **p < 0.01 versus control. Data are means \pm SEM. Each n = 6.

(C) Stimulation of NHE1 activity by 0.3 μ M PGZ in wild-type, but not in PPAR $\gamma^{-/-}$ cells.

(D) Signaling mechanism underlying the stimulation of NHE1 activity by PGZ. Actinomycin D (ActD, 5 μ M) was added to the medium for 1.5 hr prior to pHi measurements. Open bars represent the control activities and closed bars represent the activities in the presence of 0.3 μ M PGZ. **p < 0.01 versus control. Data are means \pm SEM of six to seven experiments.

(E) ERK phosphorylation in EF cells. Cells were incubated in the absence or presence of inhibitors for 40 min and 0.3 μ M PGZ was added for 5 min. GW; GW9662. AG; AG1478. See also Figure S4.

partially, in TZD-induced volume expansion. Interestingly, the Src-dependent Na/K pump activation by ouabain is dependent on the NHE1 activation (Holthouser et al., 2010). It remains to be determined whether the NHE1 activation plays a similar role in the stimulation of PT transport by TZDs.

Although TZDs are known to trigger diverse rapid cellular signaling events including the activation of kinase signaling pathways such as phosphatidylinositol 3-kinase (PI3K)/Akt, ERK, EGFR transactivation, the production of reactive oxygen species, or Ca²⁺ influx (Burgermeister and Seger, 2008), the mechanisms underlying such dose-, time-, and cell type-dependent responses have been largely unknown. The kinetics of responses, the absolute requirement of ligand-binding ability, and the nonrequirement of transcriptional activity shown in this study clearly indicate that PPAR γ , like another nuclear receptor ER (Kousteni et al., 2001), can activate the ERK pathway through the nongenomic mechanism. The dependence on Src, the association between PPAR γ and Src, and the negative effect of constitutive Src activation all support the central role of Src in the PPAR γ -dependent nongenomic signaling. Src was previously shown to play a similar essential role in the ER-mediated nongenomic signaling (Li et al., 2007). Subpopulations of ER and/or a truncated variant of ER localized to specialized membrane rafts caveolae are associated with several signaling molecules, including Src and eNOS (Li et al., 2003). Interestingly, PPAR γ is also associated with caveolin-1 (Burgermeister et al., 2003), raising the possibility that a subset of PPAR γ , together with other scaffold and signaling molecules including Src, may form a membrane-localized signaling complex that is responsible for the nongenomic actions. Also, it could be possible that the direct association of PPAR γ and MEK (Burgermeister and Seger, 2008) is involved in this signaling complex.

In contrast to the PPAR γ -dependent stimulatory effects of submicromolar concentrations of TZDs, suprapharmacological concentrations of TZDs inhibited the NHE1 activity independently of PPAR γ . Higher micromolar concentrations of TZDs were known to induce other cellular responses including capacitive calcium entry or rapid cellular acidosis, and such drastic changes in cellular homeostasis could even result in PPAR γ -independent ERK activation (Dewar et al., 2007; Friday et al., 2007). Thus, caution is required when acute in vitro responses to higher micromolar concentrations of TZDs are to be analyzed in the absence of ambient proteins. Notably, the protein-unbound peak plasma concentrations of TZDs in human subjects are estimated to be at submicromolar levels (Deng et al., 2005; Krieter et al., 1994), well within the stimulatory range for PT transport.

Our study confirmed that important species differences exist in the mechanism of TZD-induced fluid retention. The studies on collecting duct-specific PPAR γ -deficient mice indicate that the distal nephrons play a central role in TZD-induced volume expansion in mice (Guan et al., 2005; Zhang et al., 2005). While the role of ENaC is recently called into question, TZDs may enhance the expression of other sodium and fluid transporters through the classical genomic action of PPAR γ (Vallon et al., 2009). The lack of TZD-induced transport stimulation in mice PTs shown in the present study also supports the central role of distal nephrons in TZD-induced volume expansion in mice, though the actual transporter responsible for the enhanced reabsorption in distal nephrons still remains to be determined. On the other hand, several lines of evidence suggest that the transport stimulation in distal nephrons alone cannot explain TZD-induced volume expansion in species other than mice. For example, amiloride failed to prevent the PPAR γ agonist-induced volume expansion in rats (Chen et al., 2005).